ELSEVIER

Contents lists available at ScienceDirect

Journal of Terramechanics

journal homepage: www.elsevier.com/locate/jterra



Tire-ice model development for the simulation of rubber compounds effect on tire performance



Hoda Mousavi*, Corina Sandu

Terramechanics, Multibody, and Vehicle Systems (TMVS) Laboratory, Department of Mechanical Engineering, Virginia Tech, Blacksburg, VA 24061, United States

ARTICLE INFO

Article history: Received 10 February 2020 Revised 13 May 2020 Accepted 2 June 2020

Keywords:
Tire modeling
Tire-ice model
Dry friction
Viscous friction
Water film
Tread rubber compound

ABSTRACT

The material properties of the rubber compounds, which are highly dependent on temperature, have a vital role in the tire behavior. A comprehensive study on the effect of the rubber properties on tire performance, for different temperatures, as well as different road conditions is required to adequately predict the performance of tires on ice.

In this study, a theoretical model has been developed for the tire-ice interaction. The temperature changes obtained from the model are used to calculate the height of the water film created by the heat generated due to the friction force. Next, the viscous friction coefficient at the contact patch is obtained. By using the thermal balance equation at the contact patch, the dry friction is obtained. Knowing the friction coefficients for the dry and wet regions, the equivalent friction coefficient is calculated. The model has been validated using experimental results for three similar tires with different rubber compounds properties. The model developed can be used to predict the temperature changes at the contact patch, the tire friction force, the areas of wet and dry regions, the height of the water film for different ice temperatures, different normal load, etc.

© 2020 ISTVS. Published by Elsevier Ltd. All rights reserved.

1. Introduction

Tire design involves a deep understanding the effect of each tire parameter on its performance and, in general, on the vehicle control and stability. Such knowledge helps a manufacturer improve tire performance for specific operational conditions. Several past studies have been dedicated to identifying the parameters with the highest effect on tire performance. In (Mashhadi et al., 2015), the effect of different tire physical parameters on tire performance was investigated using finite element modeling (FEM). Considering the effect of contact patch properties on tire performance, the influence of different operational parameters, such as slip ratio, on the tire performance has been investigated in other studies, such as (Liang et al., 2019). Research has also been conducted to investigate the effect of different tire parameters on its performance on ice (Bhoopalam et al., 2014, Bhoopalam et al., 2015, Bhoopalam et al., 2016, Savitski et al., 2017, Jimenez and Sandu, 2018). In (Mousavi et al., 2019), several tests have been performed to investigate the effect of parameters, such as normal load and inflation pressure on the frictional forces of free rolling tires.

E-mail addresses: hoda13@vt.edu (H. Mousavi), csandu@vt.edu (C. Sandu).

In another experimental study on the tire-ice interaction has been conducted (Ivanovic et al., 2006), the effect of parameters, such as vehicle speed and tire forces, on the friction dynamics in the contact patch has been investigated. In (Makkonen and Tikanmäki, 2014) it has been shown that for very low vehicle speed and very cold ice temperature, dry friction occurs in the tire-ice contact area. In (Roberts, 1981), the researchers investigated the influence of tread compounds on tire-ice friction by focusing on the effect of the glass transition temperature for an icy road at different temperatures.

By increasing the temperature at the contact patch, especially for the temperature close to the melting temperature of ice, a water film will be produced on the top of the ice by the heat generated as a result of the frictional force. This water film can cause a change in the nature of the friction from completely dry to a combination of viscous/wet and dry friction or only to viscous friction. Several parameters, such as the ice temperature, the slip ratio, the ambient temperature, and the rubber compounds of the tire, can influence the height of the water film.

In an experimental study (Gießler et al., 2010) the effect of ambient temperature on tire-ice interaction has been investigated and it has been shown that increasing the ambient temperature will increase the water film created. As the height of the water film on the surface is one of the parameters that influence the most the

^{*} Corresponding author.

Nomenclature Longitudinal slip ratio Roughness parameter in longitudinal direction, [mm] κ_{x} k Thermal conductivity of the rubber, [W/m·K] Sliding velocity, [m/s] C_p ΔT Pressure applied on the rubber block, [mm] Specific heat of the rubber, [J/kgK] P_{nom} Temperature rise, [°C] Viscosity of the ice, [mm] η F_{Z} Normal load on the tire, [N] Density of the ice, [kg/m³] ρ F_X Longitudinal force, [N] Thermal conductivity of ice, [W/m·K] λ Longitudinal velocity at the axle of wheel, [m/s] C Specific heat of ice, [J/kgK] Е L Latent heat of the ice, I/kg Modulus of elasticity of rubber, MPa T_{m} Melting temperature, [°C] h(x)Height of the water film, [mm] T_{ice} Ice temperature, [°C] $\langle D \rangle$ Average contact diameter R Radii of the spherical asperities, [mm] ∇z Mean root square gradient Roughness parameter of rubber, [mm] 1 Wheel angular speed, [rad/s] ω

magnitude of the viscous friction, in order to fully understand the tire-ice interaction, it is important to find a way to predict the height of the water film. A theoretical model has been developed by Wiese et al. (2012) in order to estimate the viscous friction coefficient for a sample rubber block. In this study, the rubber block is in contact with ice. According to their results, rubber samples with different compounds show different behavior when they are in contact with ice. The magnitude of the frictional force is different for each rubber compound.

In the present study, the main objective is the investigation on the effect of different tire-ice parameters such as the material properties of the tread on tire performance on ice. To achieve this objective, a theoretical model has been developed in order to predict the friction coefficient and also the height of the water film created for the different tires. The developed model, ATIIM2.0, is a combined and improved version of the previous models TIM, (Bhoopalam et al., 2016) and ATIIM, (Jimenez and Sandu, 2019), from TMVS laboratory at Virginia Tech. The new model is able to predict the tire-ice friction at the contact patch for both dry and wet regions. The simulation results presented have been validated using the data collected during a previous experimental study.

This paper includes six sections. After a brief introduction in Section 1, the input data for the new model is explained in Section 2. In Section 3, the methodology followed for the development of the new tire –ice model (ATIIM2.0) is presented. The results from the simulation are shown in Section 4. Section 5 includes a brief explanation of the experimental approach to study the effect of rubber compounds on tire performance. Some experimental results are presented in this section too. A brief summary of the simulation results and the conclusions of the study are discussed in Section 6.

2. ATIIm2.0 input data

ATIIM2.0 requires several types of input data. The first input data category is related to the material properties of the tire and includes: the density (ρ) , the thermal conductivity (k), the specific heat (Cp), Young's modulus (E), the radii of spherical asperities of the rubber(R), and the roughness parameter (l) of the rubber. The required parameters have been provided by the tire company (for tire B, C, and G). According to this data, tire B has the lowest value of both Young's modulus and specific heat (Mousavi et al., 2019). Tire C has the second lowest values of these parameters.

The density of the rubber tread section of the tires B, C, and G are given as 1103 kg/m^3 , 1094 kg/m^3 , and 1137 kg/m^3 , respectively. For the roughness parameters, constant values from the literature have been chosen for all three tires (Wiese et al., 2012). The

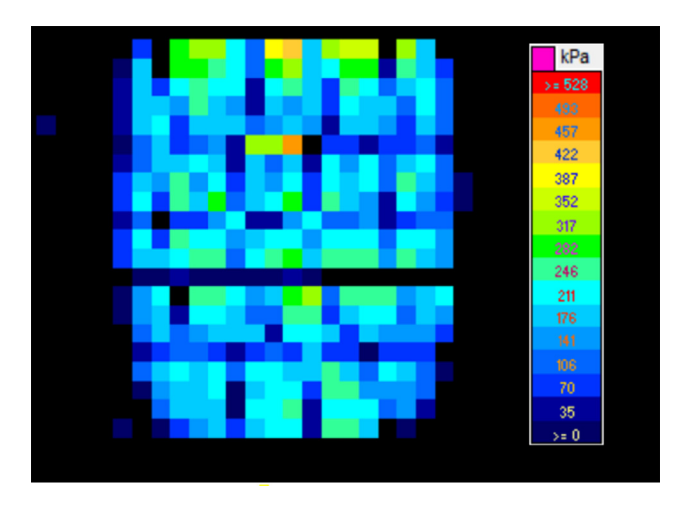


Fig. 1. Pressure distribution for tire C at 2% slip ratio.

thermal conductivity of the tread was assumed to be 0.3 W/m. K for all the tires.

The second category of the input data is related to the pressure distribution at the contact patch. ATIIM2.0 uses the value of the pressure at each point of the contact patch to predict the height of water film, as well as the friction coefficient. In order to provide this input for the model, several tests have been conducted at TMVS to collect the pressure distribution at the contact patch at different slip ratios using the TekScan Pressure Pad 3150 (Sensor, 2019). The tires have been cooled down, such as during the test the tire temperature was $-1~^{\circ}$ C. Data has been collected for traction, braking, and free rolling performance of the tires. Fig. 1 shows a sample data for pressure distribution in the contact patch for tire C at 2% slip ratio.

The last category of data used is related to the temperature changes at the contact patch. Temperature values in the contact patch have been collected using several thermocouples attached between the tire tread. These values have been used to validate the results obtained by ATIIM2.0.

3. Simulation

3.1. ATIIm2.0

The original tire-ice model (TIM) was developed by Dr. Anudeep Bhoopalam. This model consists of three main modules. Fig. 2

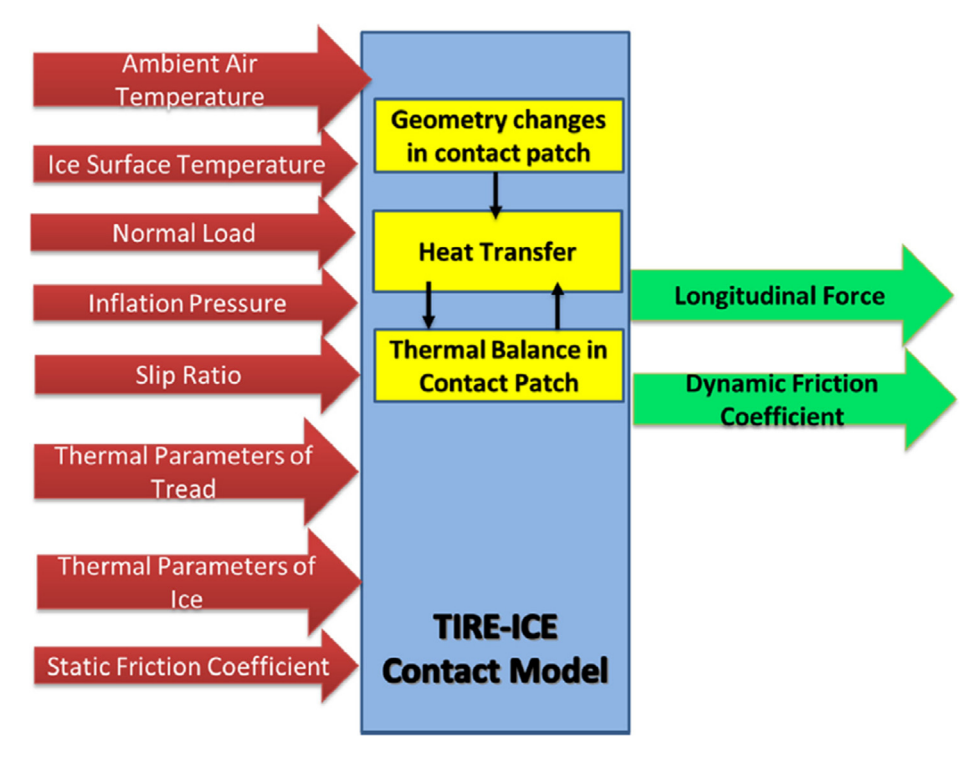


Fig. 2. Structure of the tire-ice model (TIM) (Bhoopalam et al., 2016).

shows the modular structure of the TIM. As it can be seen, the pressure distribution at the contact patch will be predicted by the first module; in the second module, the temperature rise at the contact area is calculated. By having the temperature rise at the contact patch, the average friction coefficient can be computed by the third module of the TIM. In this model, the friction coefficient can be obtained by solving the thermal balance equation at the contact patch based on the principle of heat balance, as shown in Fig. 3.

In this model, Jaeger's temperature rise formulation has been used to predict the temperature rise at the contact patch:

$$\Delta T = \frac{Q\alpha_d}{8k(\pi\alpha_d t)^{\frac{3}{2}}} exp^{\left\{-\frac{(X-x)^2+(Y-y)^2+(Z-z)^2}{4\alpha_d t}\right\}}$$
 (1)

where

$$\alpha_d = \frac{k}{\rho C_p} \tag{2}$$

k is the thermal conductivity of the rubber, C_p is the specific heat of the rubber, ρ is the density of the rubber, and ΔT is the temperature rise at point P(x, y, z) on the tread as a result of a moving heat source located at (X, Y, Z) with the magnitude of Q (Jaeger, 1942), (Fujikawa et al., 1994). This model has several pros and cons. As it will be presented in the results section, TIM is an appropriate model for modeling the friction of the tire on dry ice. However, as the governing equations do not consider the water film generated at the contact patch for different tire maneuvers, such as different slip

ratios or braking conditions, the results for the wet ice predicted with TIM are not as accurate as the results predicted for dry contact. In addition, this model only has three inputs for the material properties of the rubber; they are the density, the thermal conductivity, and the specific heat of the rubber. Thus, it is not a sufficiently detailed model when one wants to compare tires with different rubber compounds.

To improve the TIM, Dr. Emilio Jimenez added several moduli in order to calculate the height of the water film generated at the contact patch, according to the schematics shown in Fig. 4. This new model, now called ATIIM, can predict the viscous friction at the contact patch using the predicted height of water film.

In this model, the same approach was used to obtain the temperature changes at the contact patch as in the TIM. However, the main objective of the ATIIM was obtaining the viscous friction coefficient at the contact patch. So this model mainly focused on the wet traction, ([imenez and Sandu, 2019).

For ATIIM to obtain the height of the water film, the differential equations Eq. (3) was solved.

$$\frac{\eta v^2}{h(t)} = \lambda \frac{T_m - T_{ice}}{\sqrt{\pi \alpha t}} + \rho L \frac{dh(t)}{dt} \tag{3}$$

where v is the sliding velocity, η is the viscosity of the water, ρ , λ , α , and L are, density, thermal conductivity, and thermal diffusivity, and the latent heat of the ice, respectively, T_m is the melting temperature, T_{ice} is the ice temperature, h(t) is the height of the water film.

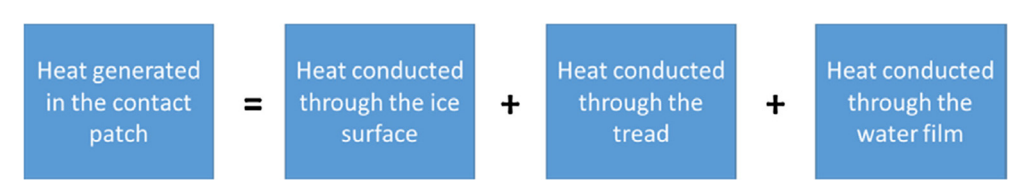


Fig. 3. Thermal balance equation at the contact patch based on the principle of heat balance (Bhoopalam et al., 2016).

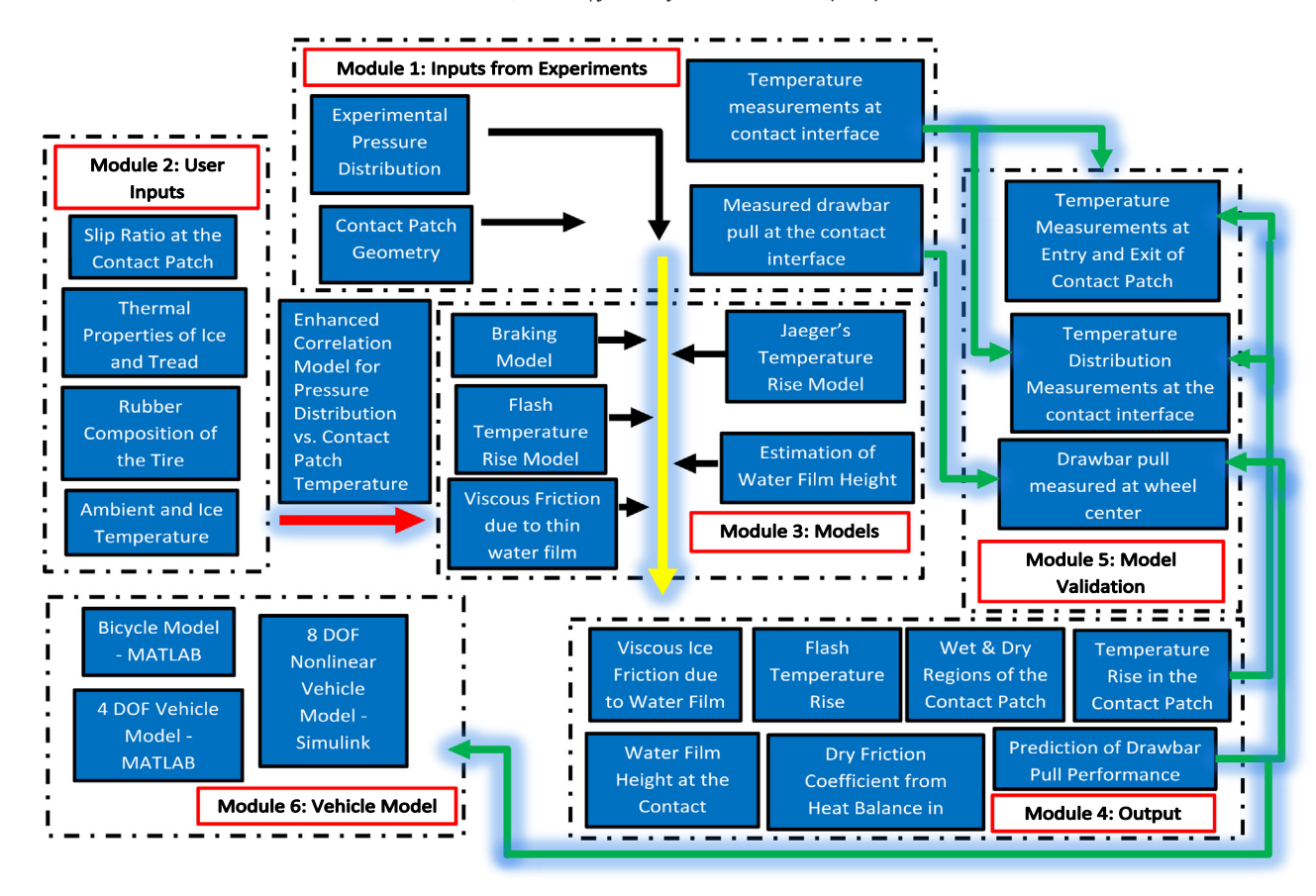


Fig. 4. Modular structure of the Advanced Tire-Ice Interface Model (Jimenez and Sandu, 2019).

Eq. (3) has three terms. The first term on the left side is the heat generation term as a result of the viscous friction coefficient. The first term on the right side is the heat transfer to ice. The second term on the right side is the energy required for melting the ice.

After finding the height of the water film, to obtain the friction coefficient Eq. (4) was used in ATIIM.

$$\mu = \frac{\eta v \kappa}{h(t) P_{nom}} \tag{4}$$

Parameter K in this equation is the apparent contact area and P_{nom} is the pressure applied on the rubber block.

Although the presented results by ATIIM show that this model is an appropriate model to predict the viscous friction coefficient in the contact patch for a tire that is in contact with wet ice, this model still implements only three of the rubber compound's properties of the tire, similar to the inputs for the TIM (the density, the thermal conductivity, and the specific heat of the rubber). Thus, it still has the same disadvantage as TIM has in predicting the friction coefficient for different tires with different rubber compounds. In order to study the effect of rubber compounds on the tire performance on ice, a model that accounts for more physical and material properties was required. In addition, as the contact area includes both, dry and wet regions, to study the performance of the pneumatic tire on ice, a model that is suitable for and can accurately predict both, dry and wet friction, must be used.

To solve the problems of the prior models, in this study, ATIIM has been improved such that the new model, ATIIM2.0, can predict viscous friction for wet regions, dry friction coefficient at dry regions, and also combined friction when we have both types of regions, using several additional rubber compounds properties, such as Young's modulus (E), the radii of spherical asperities of the rub-

ber(R), and the roughness parameter (l) of the rubber. By doing so, not only a model that is appropriate for wet and dry conditions has been developed, but also, as it will be presented in the results section, the accuracy of the results has been improved compared with the previous models for tires with different rubber compounds.

In order to develop the ATIIM2.0 several sections in the modular structure of the ATIIM have been changed. One of the main changes is in the approaches used to obtain the height of the water film and the viscous friction. Using the new approaches, the new model (ATIIM2.0) has several additional inputs for the rubber thermal and mechanical properties. Considering the fact that the height of the water film can also be influenced by the effects of the roughness, in the new model, the extension of the thermodynamic equation, which can include the roughness effects, has been implemented. In this approach, a term to consider the squeeze-out phenomena have been added to the thermodynamic equation (Wiese et al., 2012).

In addition, the extended model has been passed from timedependent representation to an x-dependent one, as shown in the equation:

$$\frac{dh(x)}{dx} = \frac{\eta}{\rho L} \kappa_x \frac{v}{h(x)} - \sqrt{\frac{\lambda C}{\pi \rho L^2}} \frac{T_m - T_{ice}}{(v.x)^{\frac{1}{2}}} - \frac{8}{3\eta} \frac{P_{nom}}{\langle D \rangle^2} \frac{h(x)^3}{v}$$
 (5)

This equation describes the basic approach to model the viscous friction coefficient of rubber sliding on smooth ice. For the ATIIM2.0, this differential equation has been solved to obtain the height of the water film and consequently to obtain the viscous friction coefficient. In this equation κ_x is the roughness parameter in the longitudinal direction of motion, ν is the sliding velocity, P_{nom} is the pressure applied on the rubber block, η , ρ , λ , C are the

viscosity, density, thermal conductivity, and specific heat of the ice, respectively, L is the latent heat of the ice, T_m is the melting temperature, T_{ice} is the ice temperature, h(x) is the height of the water film, and $\langle D \rangle$ is the average contact diameter obtained using the equation:

$$\langle D \rangle \approx \frac{2}{\sqrt{\pi}} \sqrt{Rl} \approx \frac{2l}{Vz} \frac{1}{\sqrt{\pi}}$$
 (6)

where R is the radii of the spherical asperities, l is the roughness parameter of rubber, and ∇z is the mean root square gradient.

To solve the equation dimensionless, the coordinates ξ and χ have been defined:

$$\xi = \sqrt{rac{x}{x_{ref}}} \quad and \quad \chi = rac{h}{h_{\infty}}$$

where

$$h_{\infty} = \left(\frac{3\eta^2 \kappa_x \langle D \rangle^2}{8\rho L P_{nom}} v^2\right)^{1/4} \tag{7}$$

and

$$x_{ref} = \frac{1}{I_m} \left(\frac{3\rho L \langle D \rangle^2}{8\kappa_v P_{nom}} \right)^{1/2} \tag{8}$$

where I_m is the so-called melting index:

$$I_{m} = \frac{\pi \eta L}{\lambda C} \kappa_{x} \frac{v^{2}}{\left(T_{m} - T_{ice}\right)^{2}} \tag{9}$$

Using the dimensionless coordinates, the first-order differential Eq. (7) becomes:

$$\frac{I_m d\chi(\xi)}{2\xi d\xi} = \frac{1}{\chi(\xi)} - \frac{1}{\xi} - \chi(\xi)^3$$
(10)

As there is no explicit analytical solution for this equation, an approximate solution has been used.

The following equation can be written for the viscous friction coefficient due to the existence of the asymptotic height of the water film h_{∞} :

$$\mu_{\infty} = \frac{\eta v \kappa}{h_{\infty} P_{nom}} \tag{11}$$

As it can be seen, the friction coefficient is dependent on the height of the water film, the pressure in the contact patch, the sliding speed, and also the parameter κ that is dependent on the modulus of elasticity E and the mean root square gradient ∇z , κ is also known as the relative real contact area and can be obtained by:

$$\kappa = 1 - e^{-3.325 \left(\frac{P_{nom}}{E^* \nabla z}\right)} \tag{12}$$

where E^* is the modulus of elasticity.

$$\kappa = \kappa_{x} \kappa_{y} \tag{13}$$

where κ_x and κ_y are the roughness parameters in longitudinal and lateral directions, respectively.

By solving the equation using an approximate solution method, the friction coefficient can be obtained:

$$\mu = \frac{2\mu_{\infty}}{\xi_a^2} (I_1 + I_2 + I_3) \tag{14}$$

where

$$\xi_a = \sqrt{\frac{a}{\chi_{ref}}} \tag{15}$$

and a is the length of the rubber blocks. For the first term of this equation (I_1) we have:

$$I_1 = \frac{\chi_{QLL}(0)}{2u_1^2} \tag{16}$$

$$\chi_{QLL}(0) = f \frac{h_{QLL}}{h_{co}} \ll 1 \tag{17}$$

where the unknown factor f has been chosen, such that 0 < f < 1. h_{QLL} is the so-called quasi-liquid water layer that is created as a result of ice surface exposure to the environment even if the temperature is below the melting temperature Tm.

$$h_{OLL}[nm] = 34 - 21.log(T_m - T_{ice})$$
 (18)

 u_{+} is depend on the melting index and can be obtained using the following equation:

$$u_{+} = \frac{\sqrt{1 + 2I_{m}} - 1}{I_{m}} \tag{19}$$

For the second and third term in Eq. (14) we can write:

$$I_2 = \frac{1}{u_+^2} ((1 - u_+)^{\frac{1}{4}} - \chi_{QLL}(0))$$
 (20)

$$I_{3} = \frac{\chi(\chi^{4} - 5)}{8(\chi^{4} - 1)^{2}} + \frac{3}{32} ln \left| \frac{\chi + 1}{\chi - 1} \right| + \frac{3}{16} arctan \chi \left| \begin{array}{c} \chi = \chi_{a} \\ \chi = \chi_{2} \end{array} \right.$$
 (21)

where

$$\chi_2 = (1 - u_+)^{1/4} \tag{22}$$

As described, by changing the approach, (Wiese et al., 2012), to obtain the water film and the viscous friction coefficient in ATIIM2.0, rubber parameters have been incorporated into the model. These parameters are E (Young's Modulus), ∇z , which is the mean root square gradient, and l (the roughness parameter of rubber). In this study, as there was not enough information for the roughness parameters of the tread of the tires used in the experimental part of this research, the constant values of $\nabla z = 0.35$ and l = 6.5 μm have been used for all three tires.

After finding the viscous friction for the wet area, the dry friction in the dry area has been calculated. The principle of thermal balance is employed here in order to compute the average friction coefficient in the tire contact patch for the dry regions. Based on the previous work, (Peng et al. 2000), the heat generated in the contact patch due to the frictional mechanism at the tire–ice interface is divided into three parts. The first part is conducted through the ice surface, the second part is conducted through the tire tread, and the remaining heat diffuses through the water film if present. In the case of dry friction, as the contact patch is completely dry, the heat conducted through the water film is zero.

$$q_{generated} = \mu_{av} p_{av} VSA_{tot}$$
 (23)

$$q_{ice} = \frac{\lambda A}{d} \Delta T \tag{24}$$

$$q_{tread} = \frac{kA}{d} \Delta T \tag{25}$$

$$q_{generated} = q_{tread} + q_{ice} (26)$$

Eq. (23) represents the heat generated at the contact patch based on the average pressure at the contact patch (Bhoopalam et al., 2016). The values of the static coefficient of friction, slip ratio, and longitudinal velocity were obtained from the experimental study (Mousavi and Sandu, 2020b; Mousavi et al., 2019; Mousavi and Sandu, 2020a). The pressure value in Eq. (23) was obtained from the experimentally-obtained pressure maps.

The heat conducted through the ice surface and through the tread is represented by Eqs. (24) and (25). The depth of penetration was initially estimated in order to compute the average friction; the depth value was further modified to match the friction from the simulation and from the indoor test program.

The temperature rise (ΔT) is obtained from the temperature rise simulations for dry regions and then it is plugged into Eqs. (24) and (25). The heat balance at the dry contact patch area is represented by Eq. (26), with the only unknown being the average friction coefficient at the contact patch.

After finding the values of the dry friction coefficient and of the viscous friction coefficient, the total friction, which is a combination of the friction values for wet and dry regions, is obtained using the ratio of the contribution of each type of friction. To obtain this value, the ratio of wet region area to the total area of the contact patch has been obtained using ATIIM2.0. Next, the average value of the total friction coefficient has been obtained using the following equation:

$$\mu_{Total(avg)} = A_r.\mu_{Viscous(avg)} + (1 - A_r).\mu_{Drv(avg)}$$
(27)

where

$$A_r = \frac{\textit{Area of the wet region}}{\textit{Total area of the contact patch}} \tag{28}$$

3.2. Extension of the TIM

As mentioned earlier, the original version of the TIM can predict the friction coefficient by solving the thermal balance equation at the contact patch. However, as there is no term in this equation to consider the effect of the water film created at the contact patch, the precision of this model for the wet contact is not as high as for the dry contact.

In this study, to improve the results obtained for wet traction using the TIM, another term has been added to the thermal balance equation, in order to consider the heat absorbed by ice during the deformation from solid to liquid, called the latent heat of the ice.

$$q_f = mL \tag{29}$$

where m is the mass of the water created at the contact patch and can be obtained using the height of the water film created and the water density. As it will be presented in the results section, despite adding the latent heat term to the thermal balance equation to consider the effect of the water film and to increase the precision of the

model for wet traction, the extension of the TIM still cannot predict the friction coefficient for wet traction as accurate as ATIIM2.0 can. That may be due to several assumptions that have been considered to solve the thermal balance equations (Bhoopalam et al., 2016).

Fig. 5 shows the average friction coefficient for tires B, C, and G that has been obtained using the extension of TIM. As it can be seen, the results are in the acceptable range when compared with the experimental results. In addition, as it can be seen from Fig. 5 that the results obtained using the extension of TIM have the correct trend and indicate a decrease in the value of the friction coefficient when the wet region started to appear at the contact area, and then the friction coefficient increases with an increase in the slip ratio. However, as mentioned earlier, although TIM is an appropriate model to obtain the coefficient of friction for a dry region, since it doesn't account for enough rubber tread parameters, it cannot capture the performance for wet contact accurately. This justifies the need to have another model to obtain the viscous friction when the tire is in contact with wet ice.

4. Simulation results

In this section, the simulation results obtained using ATIIM2.0 for the study of the effect of rubber compounds on tire performance on ice are presented. Using the ATIIM2.0 and also using the material and thermal parameters of the tread compound, one can obtain the viscous, dry, and total friction coefficient in the contact patch. We conducted such simulations for all the tires used in this study. The results obtained for tire B will be presented first. Next, the results obtained for all three tires will be compared. All the parameters required for running the simulation for all three tires, is presented in Section 4.1.

4.1. Model parametrization

In general, as it is shown in Fig. 6, ATIIM2.0 required four sets of input: parameters related to the rubber material properties, those related to the ice and water characteristics, operational parameters, and inputs regarding pressure distribution data. The input parameters from the Tekscan system are the pressure map dimensions and specifications, and pressure distribution data at the contact patch, that was collected by the experimental approach for each tire at different slip ratios.

For the rubber parameters, specific heat value, Young's modulus, thermal conductivity, and density were given by the tires man-

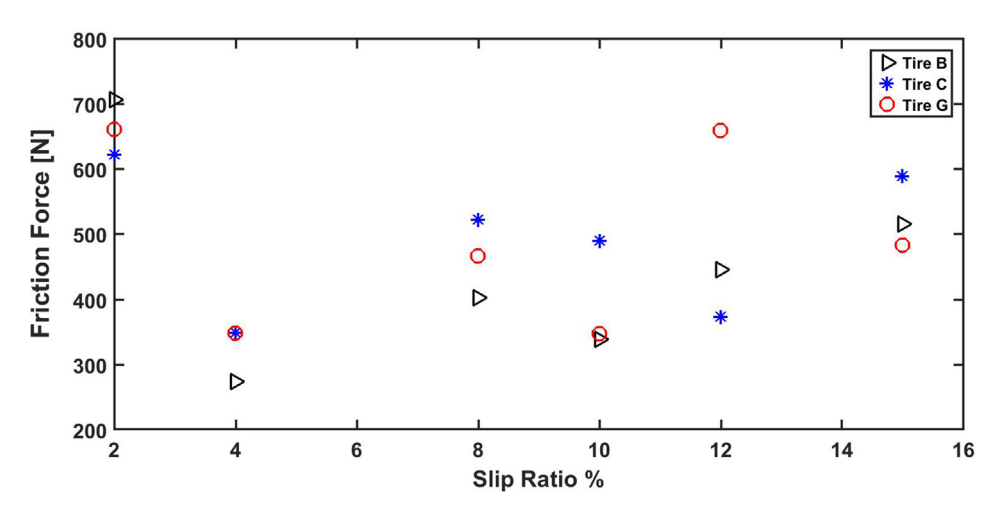


Fig. 5. Average friction force for tires B, C, and G obtained using the extension of TIM for wet and dry regions. Inflation pressure: 144.79 kPa, Nominal load: 4 kN, Ice temperature: -1 °C, Static friction coefficient ~0.1.

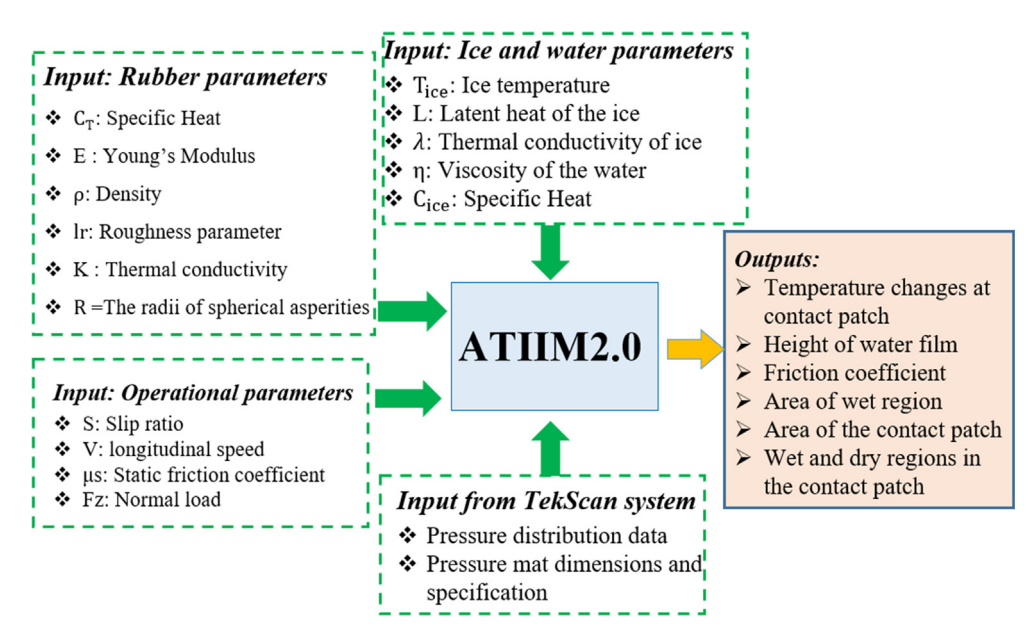


Fig. 6. Inputs and outputs of the ATIIM2.0.

ufacturer company for different temperatures (Mousavi and Sandu, 2020b; Mousavi et al., 2019; Mousavi and Sandu, 2020a). The roughness parameters Vz and I were taken from (Wiese et al., 2012). Table 1 shows the rubber inputs values for tires B, C, and G at -1 °C.

The operational values were taken from the conditions for the experimental part of this study. The normal load was 4 kN, and longitudinal speed was 0.06 m/s, which is equal to the linear speed of the Terramechanic Rig at TMVS. The static friction coefficient was equal to 0.1, which was measured before conducting the test using a slider friction tester. The slip ratio was changed from (2% to 15%).

Ice and water parameters were found at the temperature of -1 °C. The viscosity of the water is $1.787*10^{-3}$, the latent heat value is 333 kJ/kg, the specific heat of the ice is 2.027 kJ/kg K, and the thermal conductivity of the ice is 2.22 W/m K. The parameters were used from Tekscan system are the pressure distribution in the contact area which had been shown in Fig. 1 and the pressure mat dimensions. The distance between each pixel of the pressure mat is 8.4 mm. For more details for the dimensions and specification of the pressure map, please refer to (Pressure Mapping Sensor 3150).

4.2. Simulation results for traction for tire B

In this section, to show the ATIIM2.0 capabilities, one sample result from each type of possible model output is presented.

ATIIM2.0 is able to predict the distribution of the height of the water film created at the contact patch, temperature change distribution, pressure distribution, wet and dry regions at the contact area, viscous friction distribution, area of the contact patch, area

Table 1Material properties of tire B, C, and G.

	Tire B	Tire C	Tire G
C_T : Specific heat (J/kg K)	1.871*10 ³	2.126*10 ³	2.242*10 ³
E: Young's Modulus (MPa)	3.3783	4.1909	6.1419
ρ: Density (kg/m3)	1103	1094	1137
1: Roughness parameter (µm)	6.5	6.5	6.5
K: Thermal conductivity (W/mK)	0.3	0.3	0.3
abla z: The mean root square gradient	0.35	0.35	0.35

of the wet region, and also the average values for dry, viscous, and total friction coefficient, for different tire-ice conditions, such as traction and braking, different ice temperature, and different normal loads.

Fig. 7 shows the simulation results for viscous, dry, and total friction of tire B when it is in contact with -1 °C ice for a normal load of 4 kN for the slip ratio of 2%, 4%, 8%, 10%, 12%, and 15%. As it can be seen, the value of the viscous friction increased by increasing the slip ratio. This matches with the results obtained by previous studies (Bhoopalam et al., 2016), (Kandeva and Dishovsky, 2019). The increase in the values of the viscous friction is higher in the lower slip ratios range, and it tends to a constant value for higher slip ratios.

The simulation results also show that the dry friction reaches its maximum value at slip ratios around 10%. The black line in the graph shows the total friction coefficient for both regions.

In addition to the information regarding the friction coefficient, ATIIM2.0 is able to provide more data at the contact patch. Figs. 8–17 show several sample results for pressure distribution, temperature changes, the height of water film, the viscous friction coefficient distribution, and the wet and dry regions at the contact area for tire B with 4% and 12% slip ratio.

By looking at the pressure distribution in the contact patch, the larger value of pressure at the leading edge can be observed. By increasing the slip ratio, the increase in the pressure distribution in the leading edge is more visible.

As it can be seen, there is a general increase in the temperature rise from the leading edge to the trailing edge. This is due to the fact that when the tire is rolling, from the leading edge to the trailing edge, each block of rubber will be a heat source for the next block. By comparing the results for temperature rise for two different slip ratios, one can say that in general, an increasing trend can be observed in the temperature rise with the slip ratio increase.

As it can be seen from Fig. 12 and Fig. 13, there is a higher height of water film in the trailing edge of the tire. These results were expected and agreed with the results for the temperature change at the contact patch. There is more water generated when the temperature is higher. By comparing the results for two different slip ratios, one can say that the height of water film generated increases with an increase in the slip ratio.

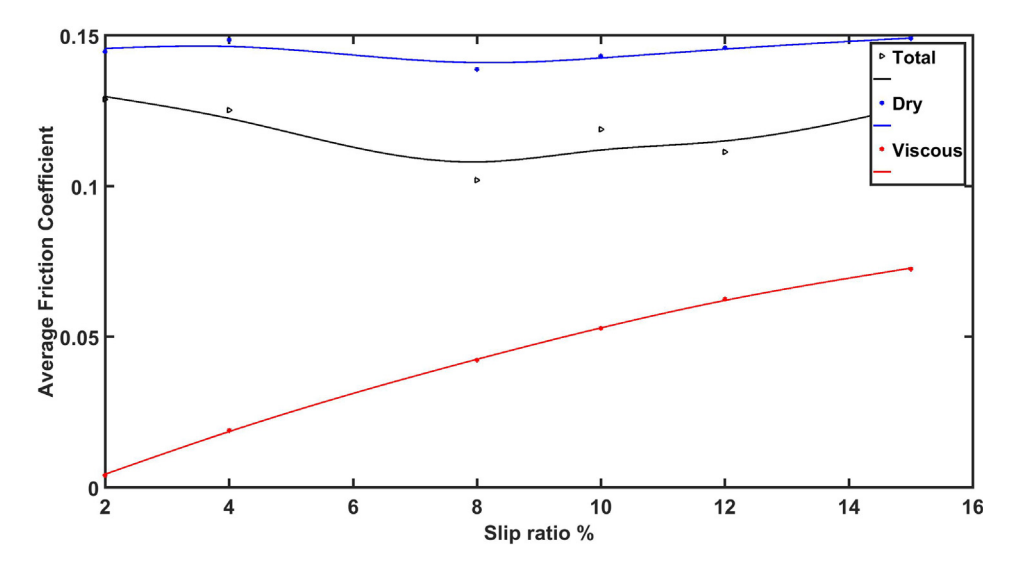


Fig. 7. Simulation results for viscous, dry and total friction of tire B.

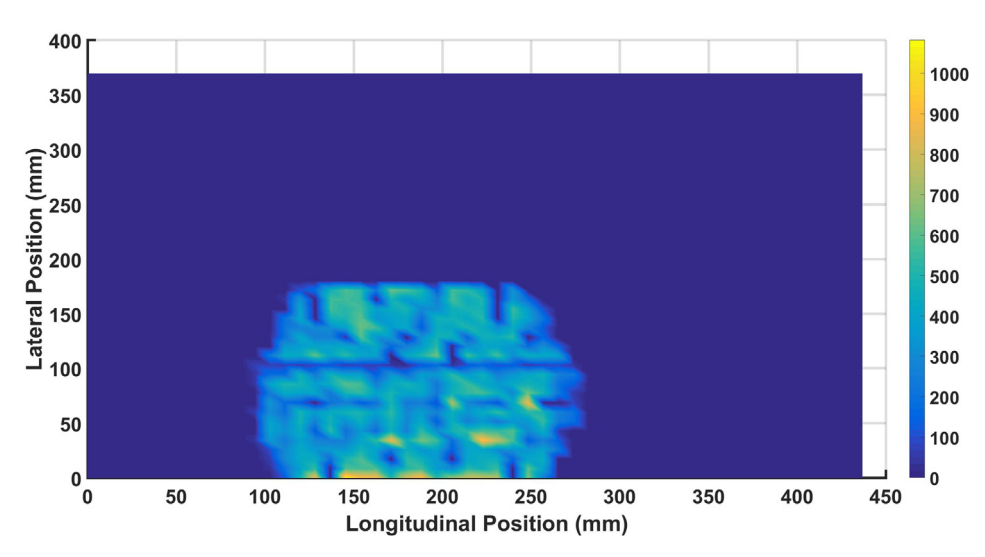


Fig. 8. Pressure distribution (Pa) in the contact patch for tire B with 4% slip ratio modeled by ATIIM2.0.

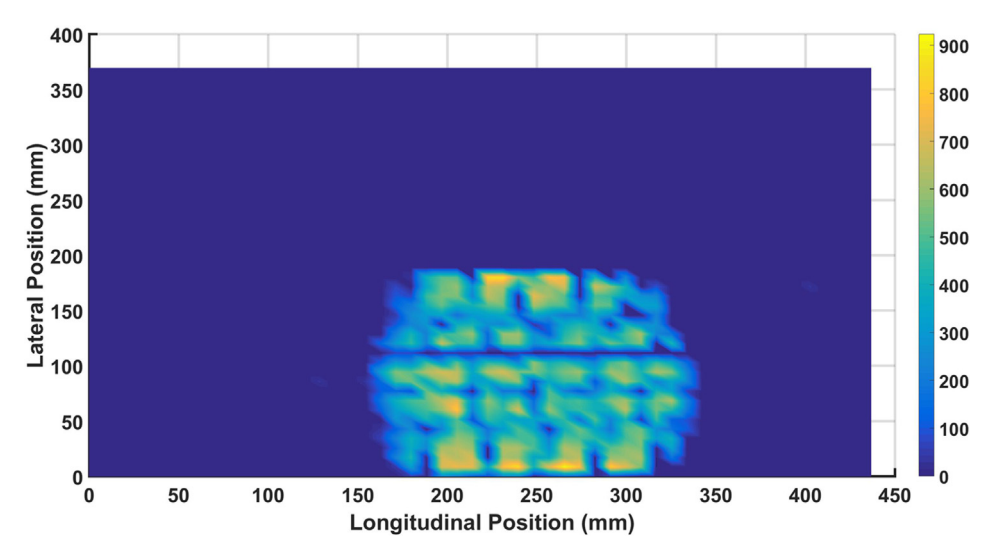


Fig. 9. Pressure distribution (Pa) in the contact patch for tire B with 12% slip ratio modeled by ATIIM2.0.

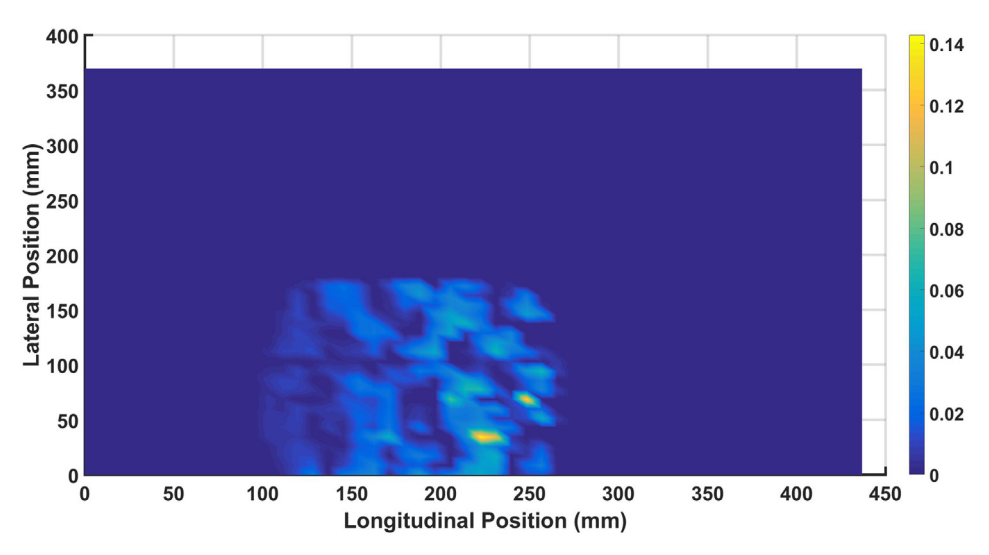


Fig. 10. Temperature rise in the contact patch for tire B with 4% slip ratio modeled by ATIIM2.0.

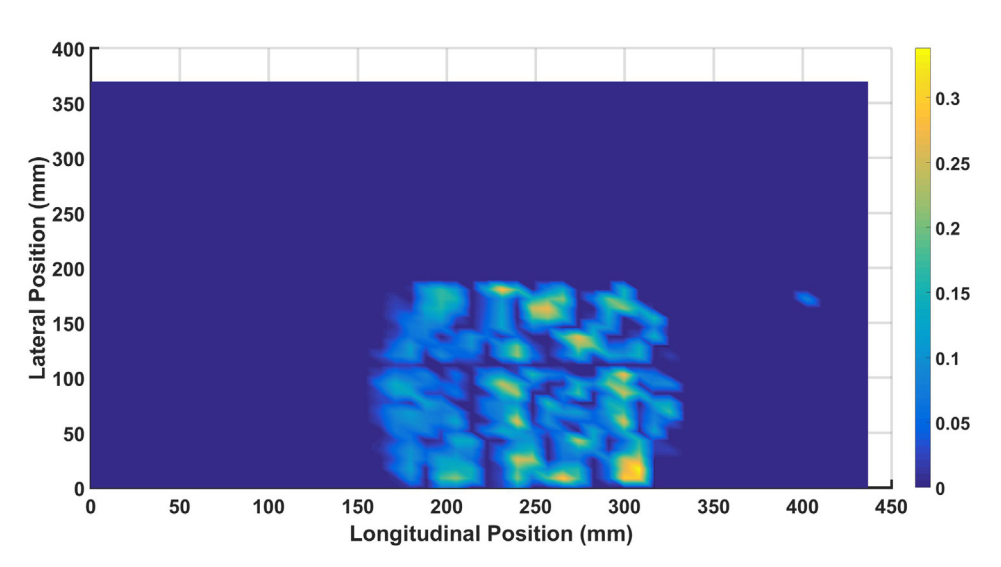


Fig. 11. Temperature rise in the contact patch for tire B with 12% slip ratio modeled by ATIIM2.

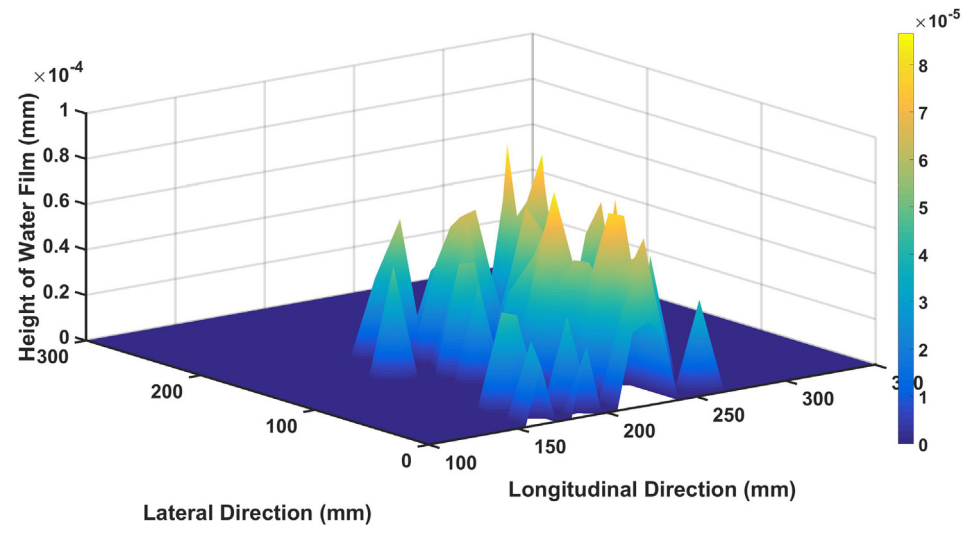


Fig. 12. Height of the water film (mm) obtained for tire B with 4% slip ratio modeled by ATIIM2.0.

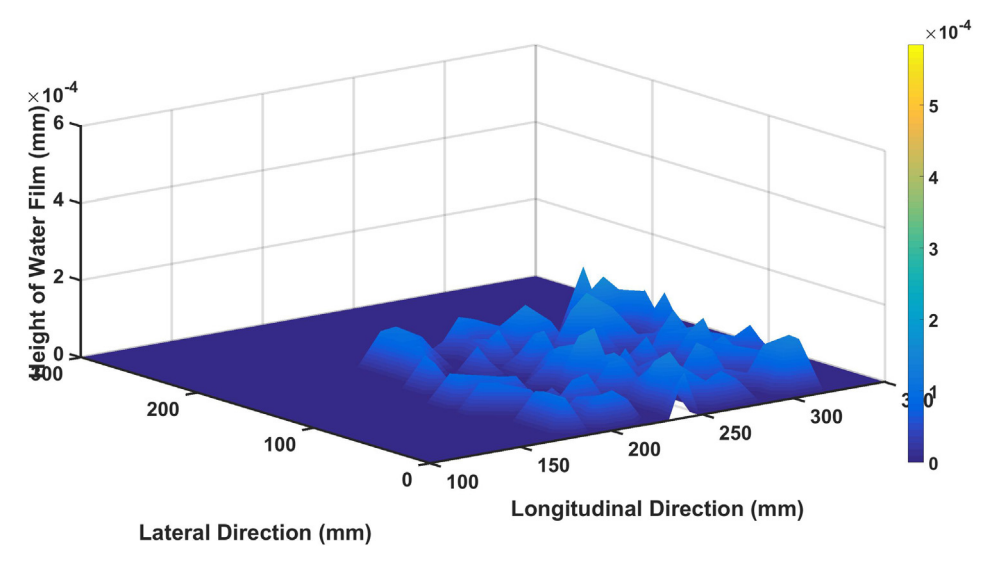


Fig. 13. Height of the water film (mm) obtained for tire B with 12% slip ratio modeled by ATIIM2.0.

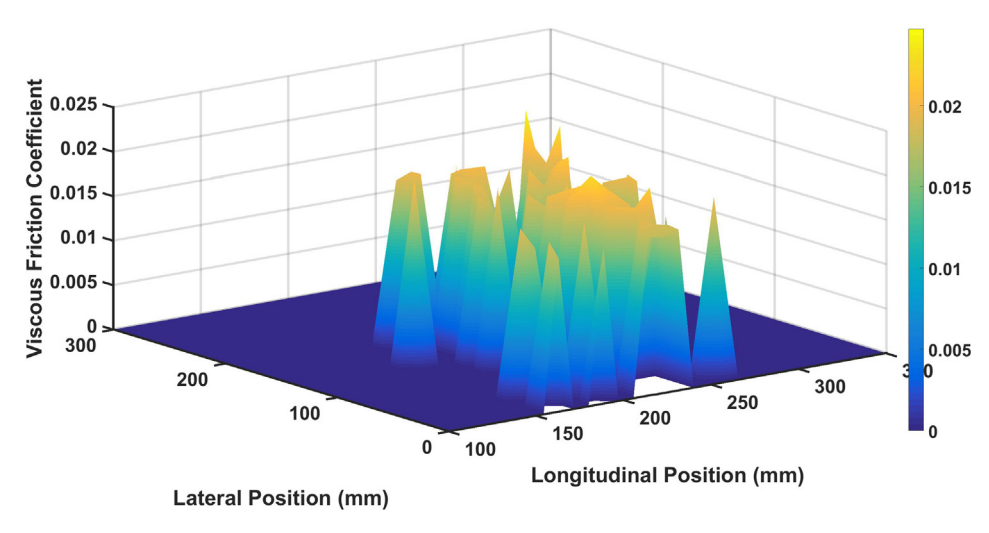


Fig. 14. Viscous friction coefficient distribution in the contact patch for tire B with 4% slip ratio modeled by ATIIM2.0.

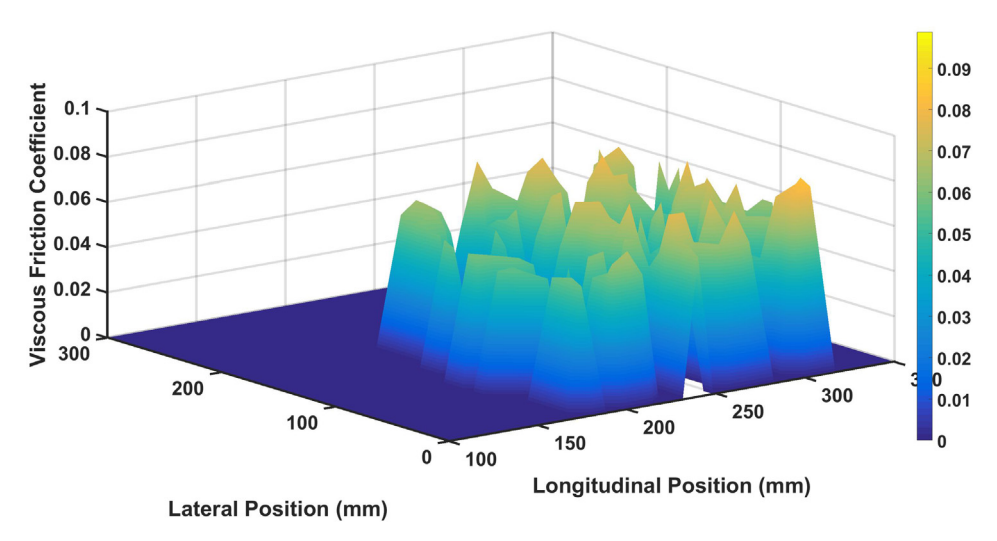


Fig. 15. Viscous friction coefficient distribution in the contact patch for tire B with 12% slip ratio modeled by ATIIM2.0.

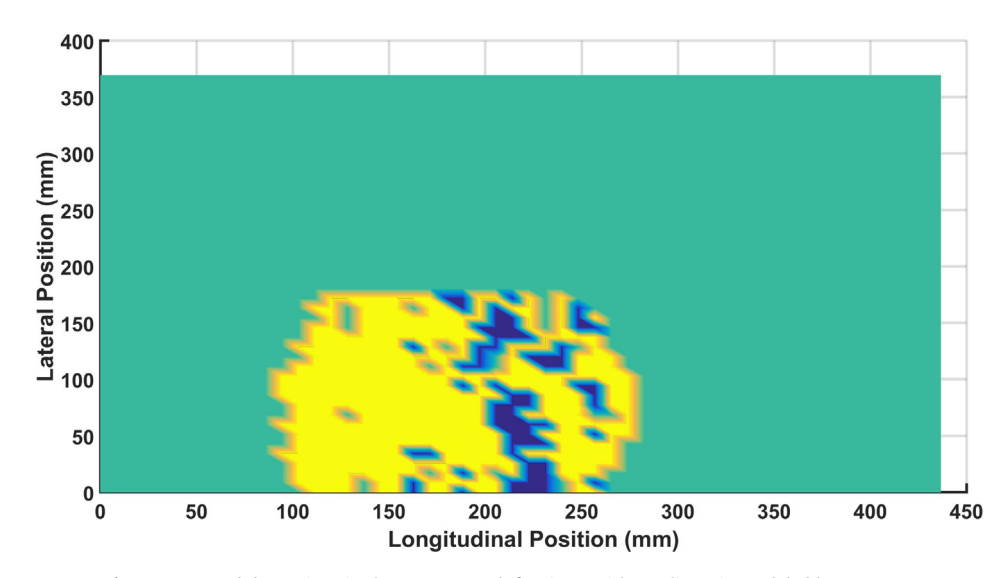


Fig. 16. Wet and dry regions in the contact patch for tire B with 4% slip ratio modeled by ATIIM2.0.

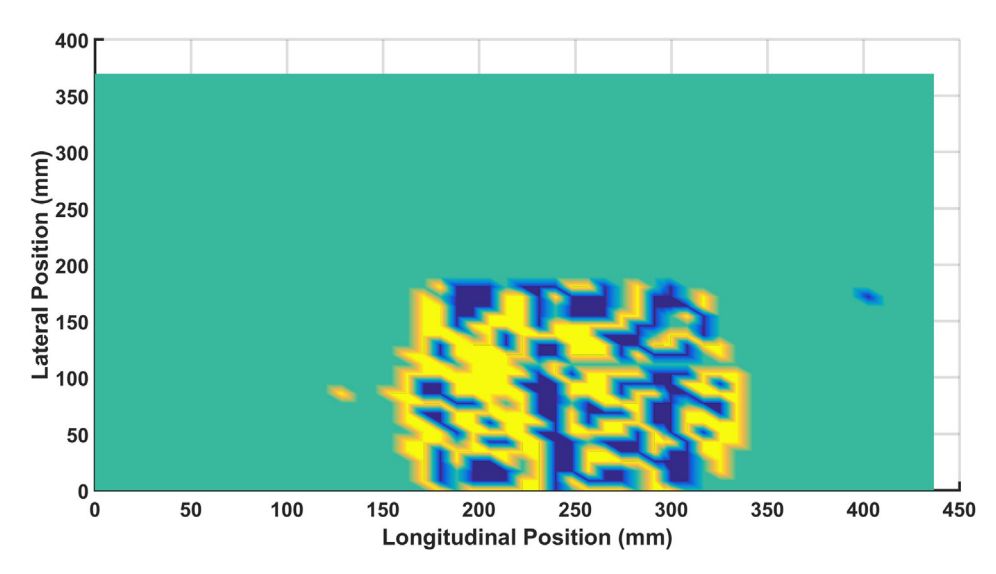


Fig. 17. Wet and dry regions in the contact patch for tire B with 12% slip ratio modeled by ATIIM2.0.

Figs. 14 and 15 show the viscous friction distribution in the contact patch. Similar to the results for the height of the water film, the value of the viscous friction coefficient is lower in the leading edge of the tire. Although considering the Eq (11) our initial expectation could have been higher values of friction for lower values of the water film height, due to the fact that in the leading edge the pressure is higher than in the trailing edge and the differences in the pressure values is larger than the differences in the water film height, the general trend is an increase in the value of the viscous friction force from the leading edge to the trailing edge. In other words, the difference in the value of the pressure negates the effect of the water film height. However, as the wet area increases from the leading edge to the trailing edge, the total friction coefficient decreases.

For two different slip ratios, again, the expectation is to obtain a lower viscous friction coefficient with an increase in the slip ratio as the height of water film will increase. However, according to Eq. (11), since the sliding velocity appears in the numerator, by increasing the slip ratio, higher values of viscous friction are in fact obtained.

The blue sections in Fig. 16 and Fig. 17 show the wet area in the contact patch. As it can be seen, there is a larger wet area when the slip ratio increases.

4.3. Simulation results for traction condition for all tires B, C, and G

In this section, the results for all three tires B, C, and G will be presented. As the thermal parameters for all three tires are different, our expectation is to obtain different results from ATIIM2.0 for each tire. In addition to the comparison among the simulation results for the three tires, the simulation results from ATIIM2.0 will be compared with data collected experimentally in our lab. The ATIIM2.0 has been used to predict the friction force for the tires B, C, and G in contact with ice at $-1~^{\circ}\text{C}$ temperature, applied normal load of 4 kN, and inflation pressure of 21 psi (60% of nominal pressure).

Considering these desired test conditions, the input values for the material and the thermal properties of the tread of each tire have been obtained using a spline method and are provided in Table 1. In addition, the data collected using the pressure mat system for different slip ratios has been used as the input for the ATIIM2.0 to obtain the pressure distribution and also temperature changes at the contact patch. Using the predicted temperature changes at the contact patch, the height of the water film and the friction coefficient were obtained for each tire.

The ATIIM (original model) was trained with data provided by Hankook Tires for the pressure distribution for the SRTT for various normal loads at various static and rolling conditions. As in this study, an in-house pressure mat was used, the new model (ATIIM2.0) had to be trained again using the new pressure mat dimensions and specifications.

Figs. 18 and 19 show the average viscous and dry friction coefficient for tires B, C, and G that have been obtained using ATIIM2.0. According to the design of the experiment, the values of the viscous and the dry friction coefficients have been obtained for the slip ratios of 4%, 8%, 10%, 12%, and 15%. Considering that the measured static friction coefficient was ~0.1, the dry friction coefficient values obtained are close to what was expected. Furthermore, previous studies indicated a general increasing trend for the viscous friction coefficients for lower slip ratios (<15%). As it can be seen, the results obtained in this study are in good agreement with past studies.

According to Fig. 18 and Fig. 19, tire B has the highest friction values for the dry and the viscous friction coefficients. Tire C has the second highest value. This result matches the results obtained experimentally for the free rolling test, which is related only to the resistive force of the tire.

Fig. 20 shows the average total friction coefficient for tires B, C and G obtained using ATIIM2.0. As it can be seen, the magnitude of the total friction coefficient is the highest for tire B. For traction, the experimental values for tires C and G are different. This may be due to several reasons. First of all, ATIIM2.0 has been developed to primarily predict the frictional force. The results obtained from the experimental traction study provided the values of the drawbar pull. In addition, as there was not enough information for the rubber roughness parameters and the thermal conductivity of the tread, the same values have been used for the simulation for all three tires. However, as it will be shown later, all these parameters play important roles in the tire performance. For more accurate simulation results, specific information regarding the thermal conductivity and the roughness parameters of the tread rubber is required for each of the tires.

4.4. Simulation results for the braking condition for tires B, C, and G

The height of water film distribution, the pressure distribution, the wet and the dry regions in the contact area, the viscous friction coefficient distribution, the average values of viscous, dry, and total friction coefficient, as well as the area of the wet region and the

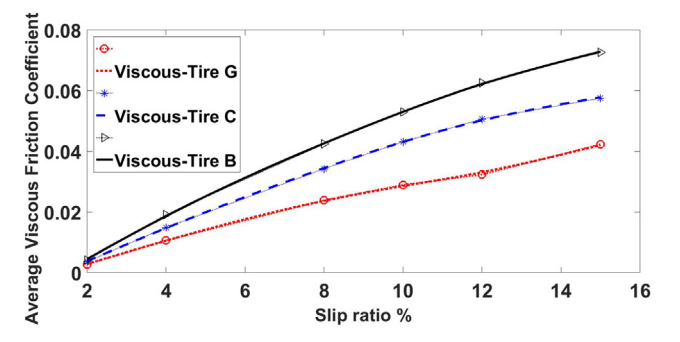


Fig. 18. Average viscous friction coefficient for tires B, C and G obtained using ATIIM2.0. Inflation pressure: 144.79 kPa, Nominal load: 4 kN, Ice temperature: -1 °C, Static friction coefficient: \sim 0.1.

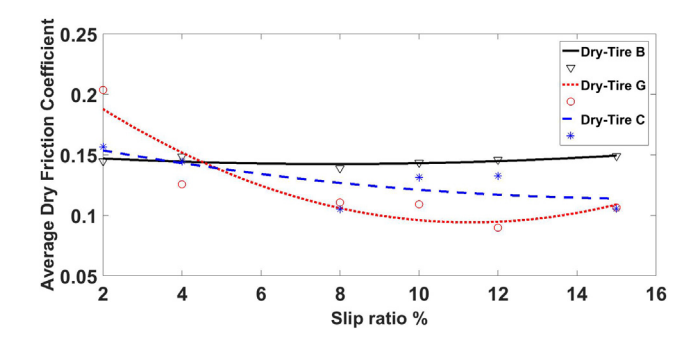


Fig. 19. Average dry friction coefficient for tires B, C and G obtained using ATIIM2.0. Inflation pressure: 144.79 kPa, Nominal load: 4 kN, Ice temperature: -1 °C, Static friction coefficient: \sim 0.1.

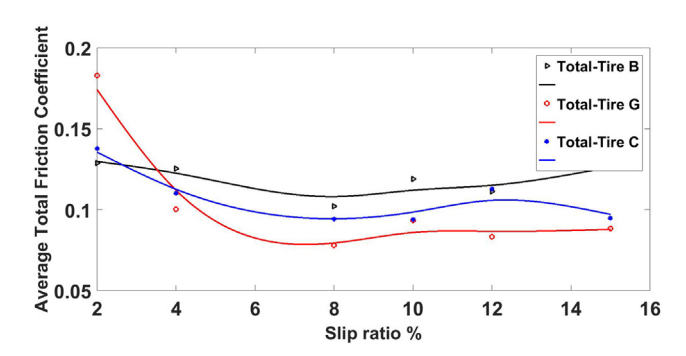


Fig. 20. Average total friction coefficient for tires B, C and G obtained using ATIIM2.0. Inflation pressure: 144.79 kPa, Nominal load: 4 kN, Ice temperature: -1 °C, Static friction coefficient: \sim 0.1.

contact patch area, have been obtained for the braking condition of tires B, C, and G using the data collected from the pressure mat and ATIIM2.0, and are presented in this section (Figs. 21–35). As it can be seen, similar to the traction condition, the height of the water film is higher at the trailing edge. We can observe higher values for the viscous friction coefficient at the trailing edge, where the pressure is lower. In general, the amount of water created during the braking condition is higher than during the traction condition.

Table 2 compares some of the values obtained from ATIIM2.0 simulations for all three tires B, C, and G for the braking condition.

As it can be seen, the viscous friction coefficient for tire B has the highest value. Tire C has the second highest value. These results match the experimental results presented in the experimental section for free rolling and braking tests. As it can be seen from Table 2, one of the advantages of tire B is having the smallest wet area in the contact patch, when compared to the other two tires.

5. Testing setup

To validate the ATIIM2.0, several tests have been conducted using the Terramechanics Rig in the TMVS Lab at Virginia Tech (Sandu et al., 2008; Khan and Sandu, 2017). The results from the experimental study have been presented in another study published by the authors (Mousavi and Sandu, 2020b; Mousavi et al., 2019; Mousavi and Sandu, 2020a). The tests were conducted for the three tires for which the simulations are presented in this study. The applied normal load and inflation pressure of the tire, the temperature of the ice, the temperature of the tire, and the percentage of slip ratio were the variables of the test. The results are presented for the braking, tractive, and free rolling conditions of the tire. Table 3 shows the design of the experiments for this study.

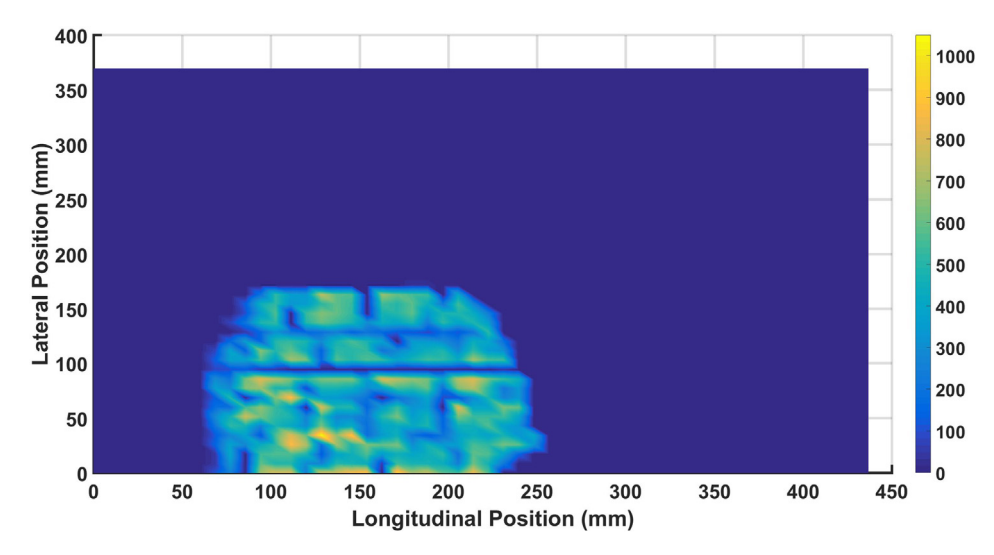


Fig. 21. Pressure distribution (Pa) in the contact patch for tire B for the braking condition, modeled by ATIIM2.0.

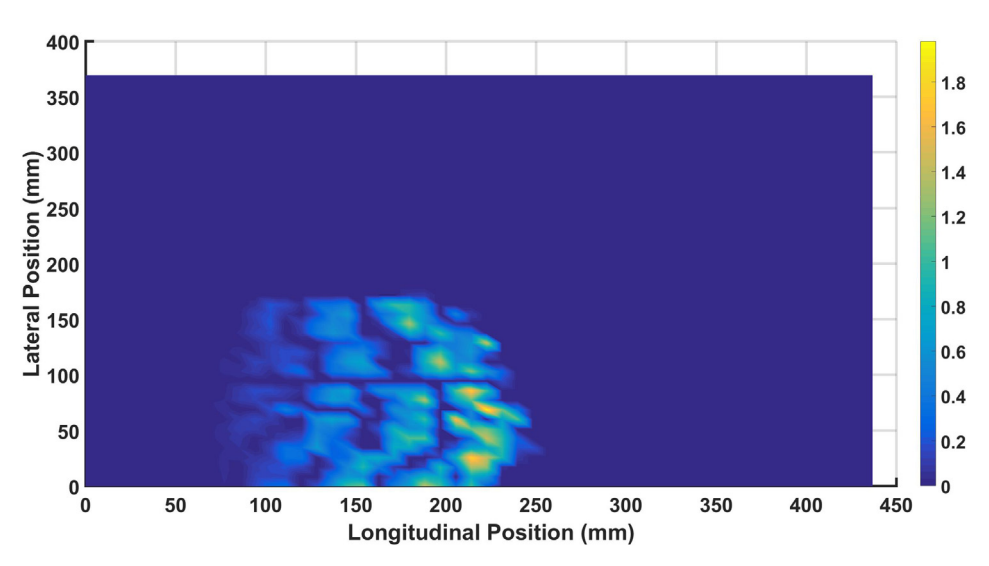


Fig. 22. Temperature rise distribution (°C) in the contact patch for tire B for the braking condition, modeled by ATIIM2.0.

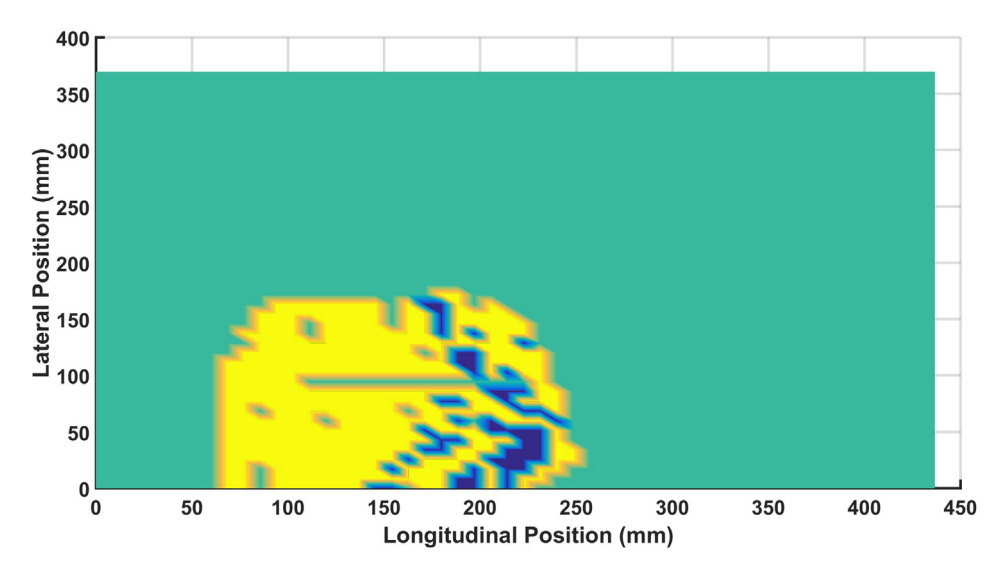


Fig. 23. Wet and dry regions in the contact patch for tire B for the braking condition, modeled by ATIIM2.0.

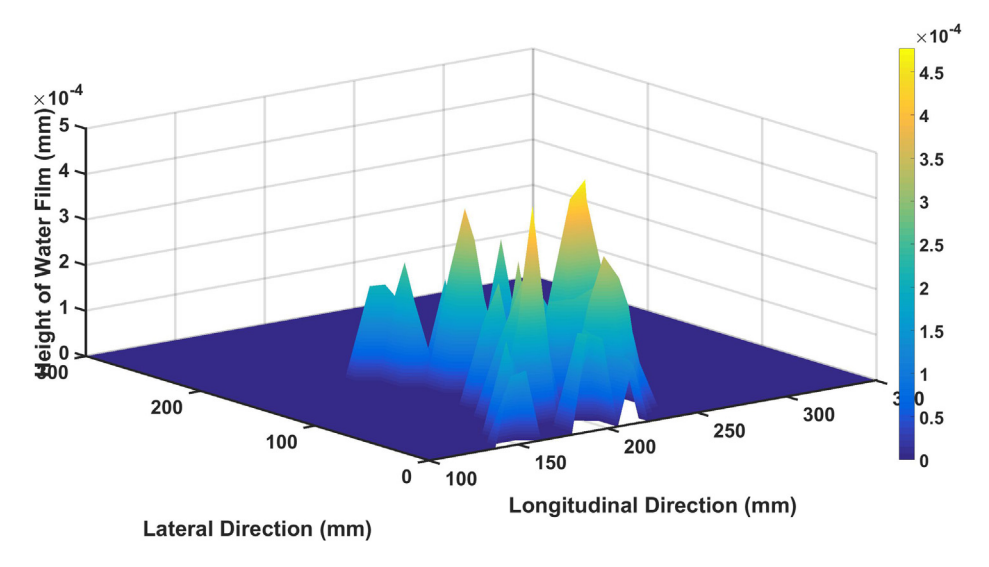


Fig. 24. Height of the water film (mm) for tire B for the braking condition, modeled by ATIIM2.0.

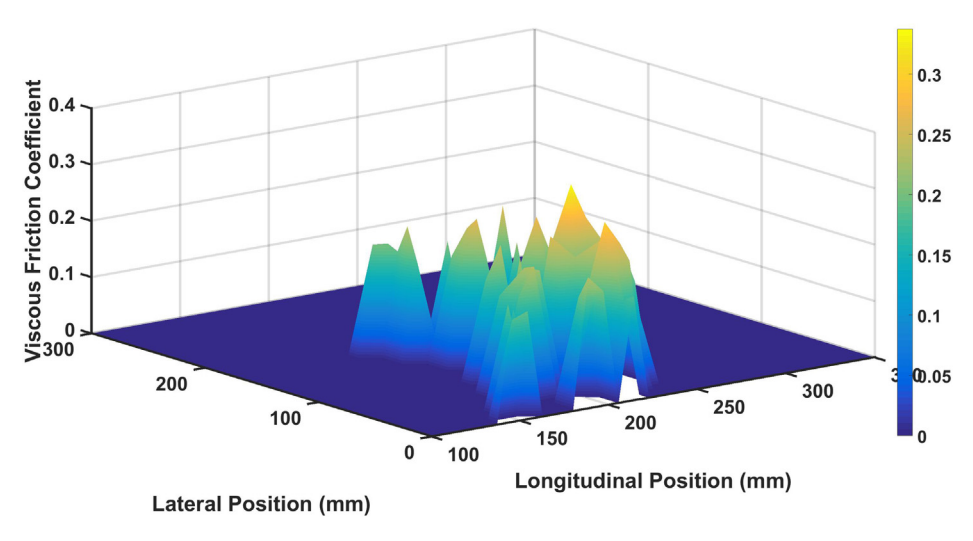


Fig. 25. Viscous friction coefficient in the contact patch for tire B for the braking condition, modeled by ATIIM2.0.

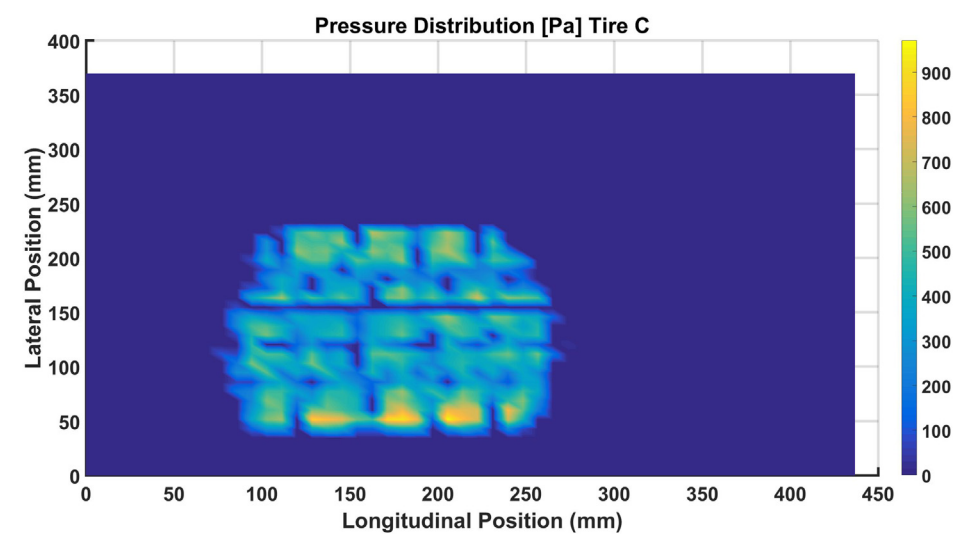


Fig. 26. Pressure distribution (Pa) in the contact patch for tire C for the braking condition, modeled by ATIIM2.0.

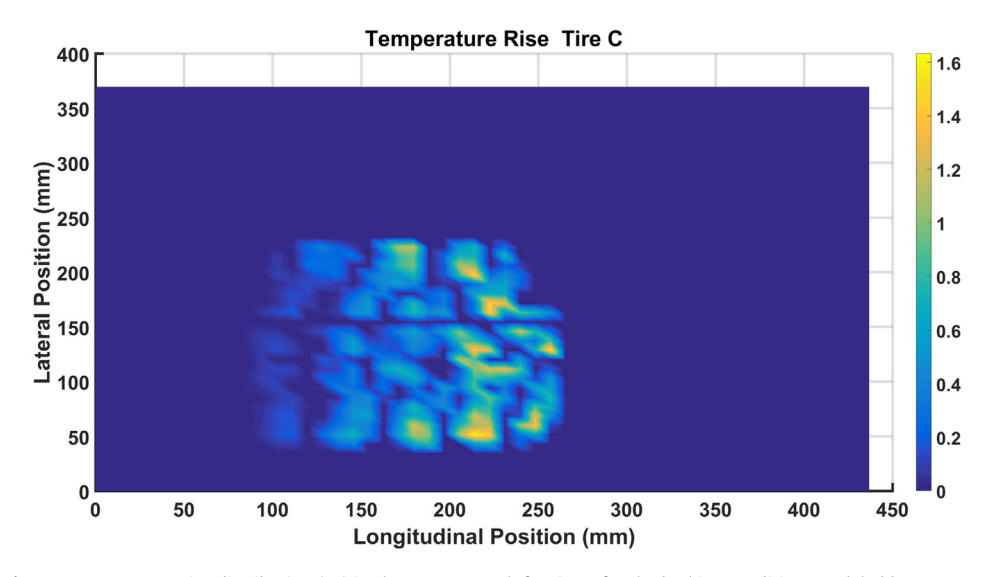


Fig. 27. Temperature rise distribution (°C) in the contact patch for tire C for the braking condition, modeled by ATIIM2.0.

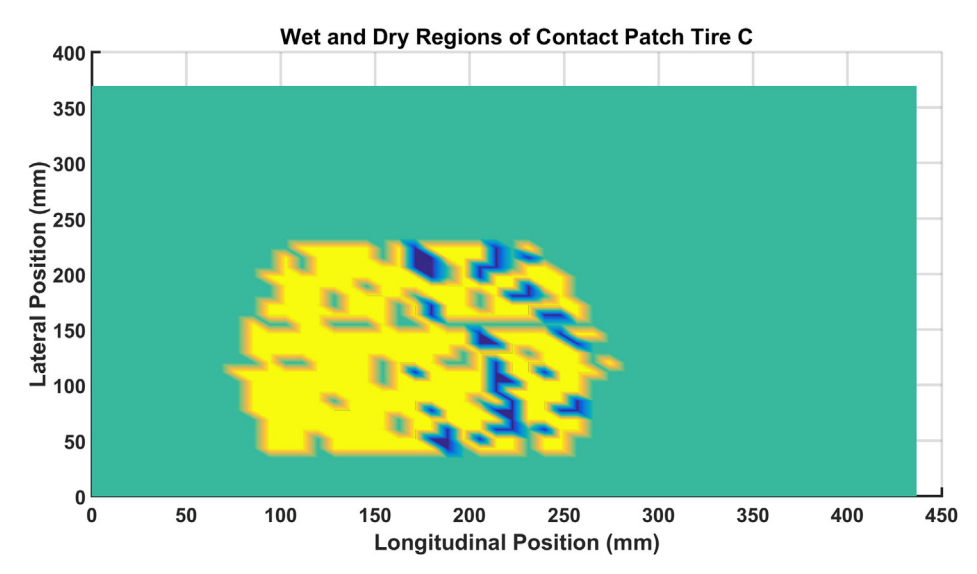


Fig. 28. Wet and dry regions in the contact patch for tire C for the braking condition, modeled by ATIIM2.0.

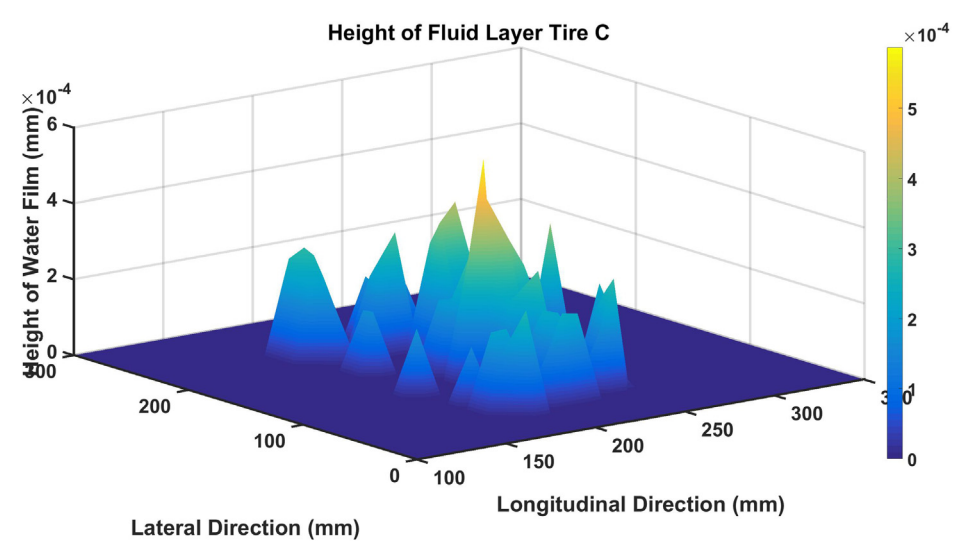


Fig. 29. Height of the water film (mm) created for tire C for the braking condition, modeled by ATIIM2.0.

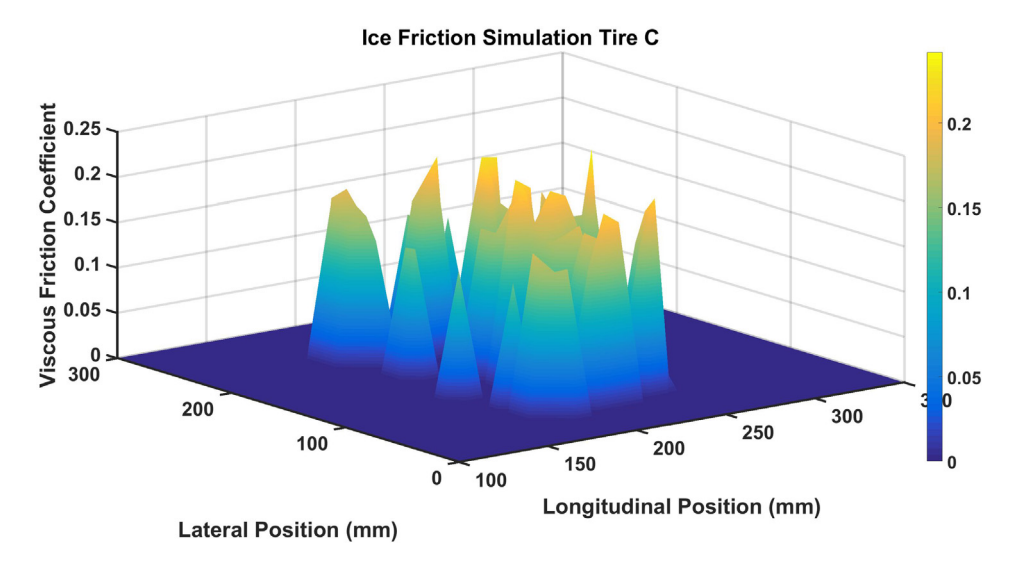


Fig. 30. Viscous friction coefficient at the contact patch for tire C at braking condition modeled by ATIIM2.0.

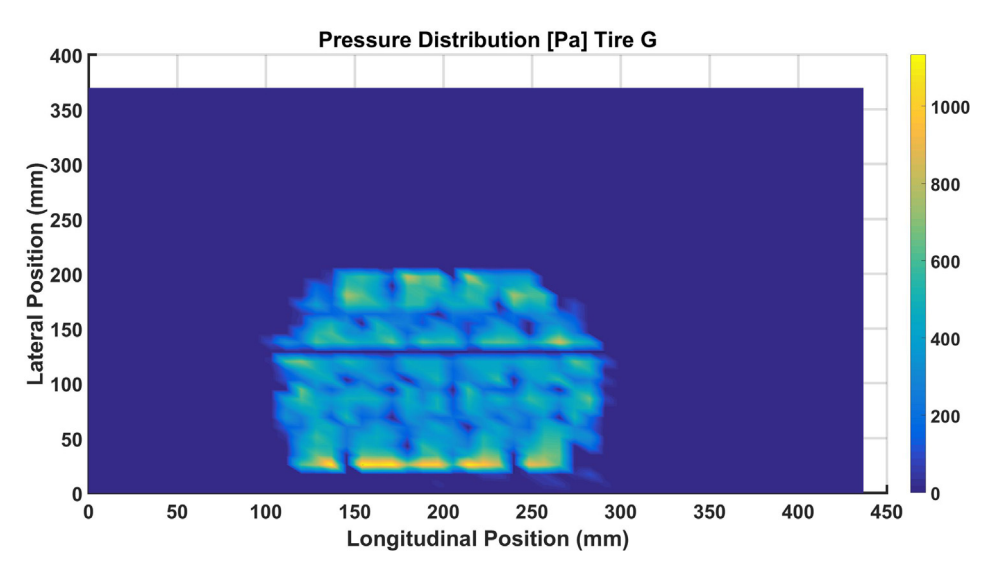
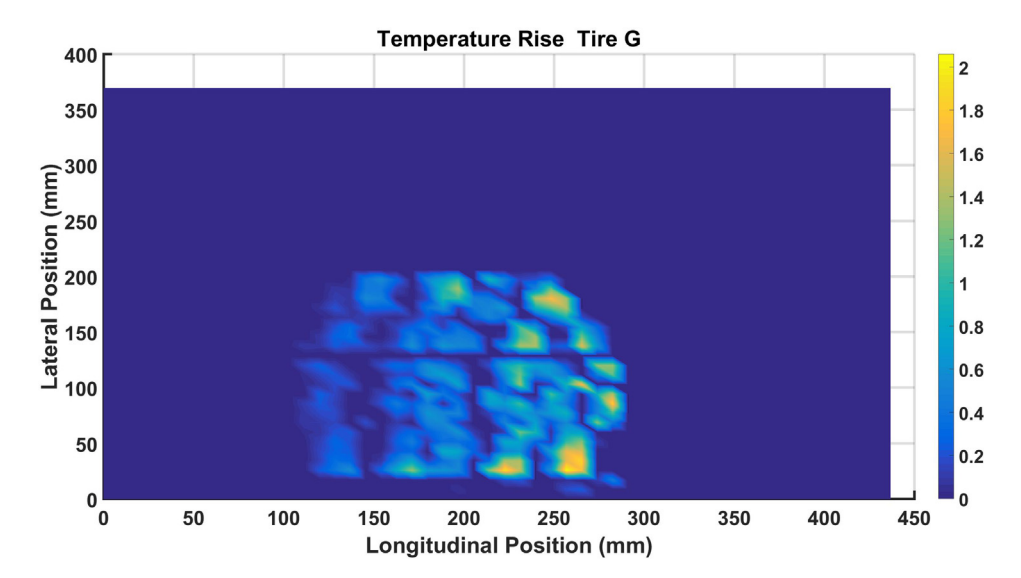


Fig. 31. Pressure distribution (Pa) in the contact patch for tire G for the braking condition, modeled by ATIIM2.0.



 $\textbf{Fig. 32.} \ \ \text{Temperature rise distribution ($^{\circ}$C) in the contact patch for tire G for the braking condition, modeled by ATIIM2.0.$

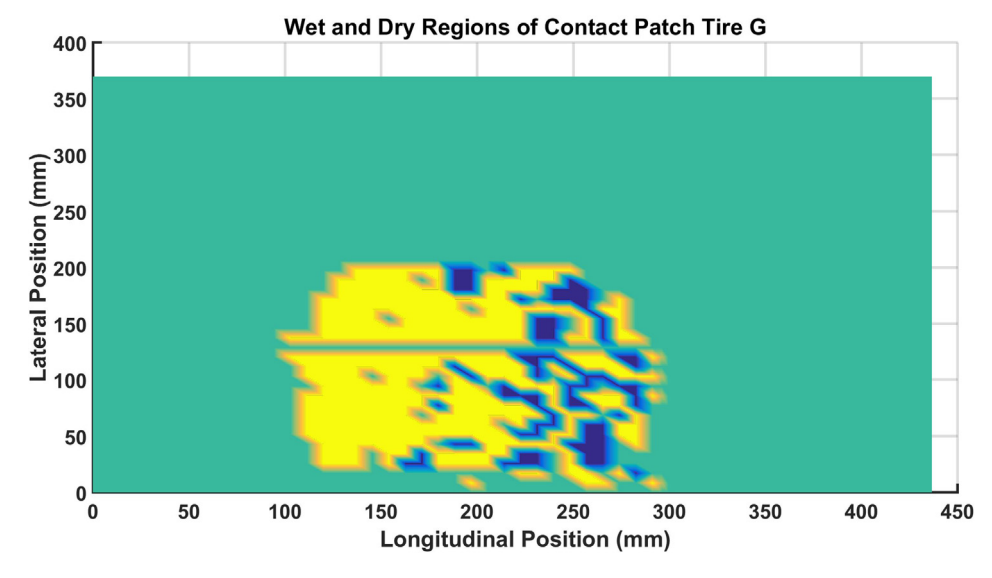


Fig. 33. Wet and dry regions in the contact patch for tire G for the braking condition, modeled by ATIIM2.0.

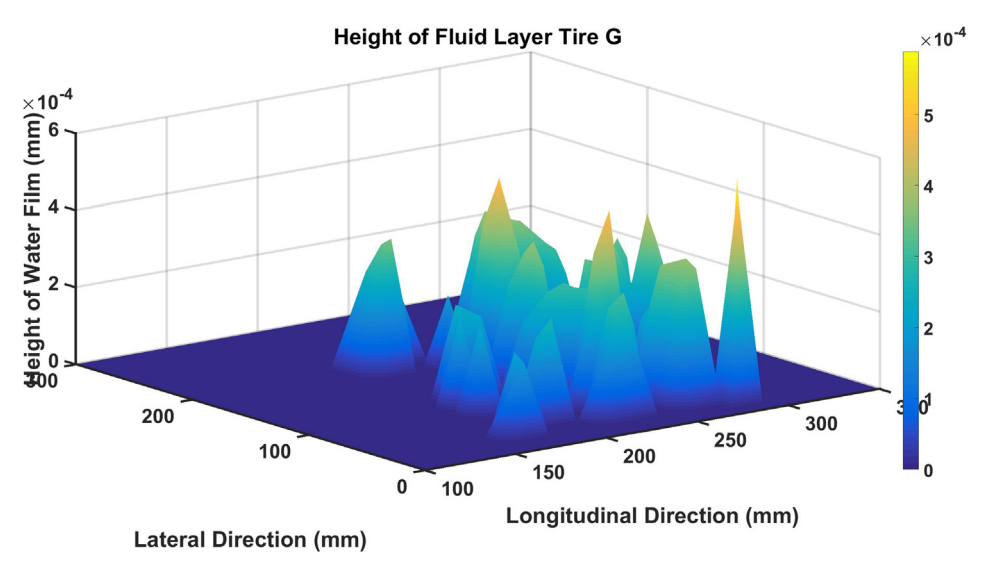


Fig. 34. Height of the water film (mm) for tire G for the braking condition, modeled by ATIIM2.0.

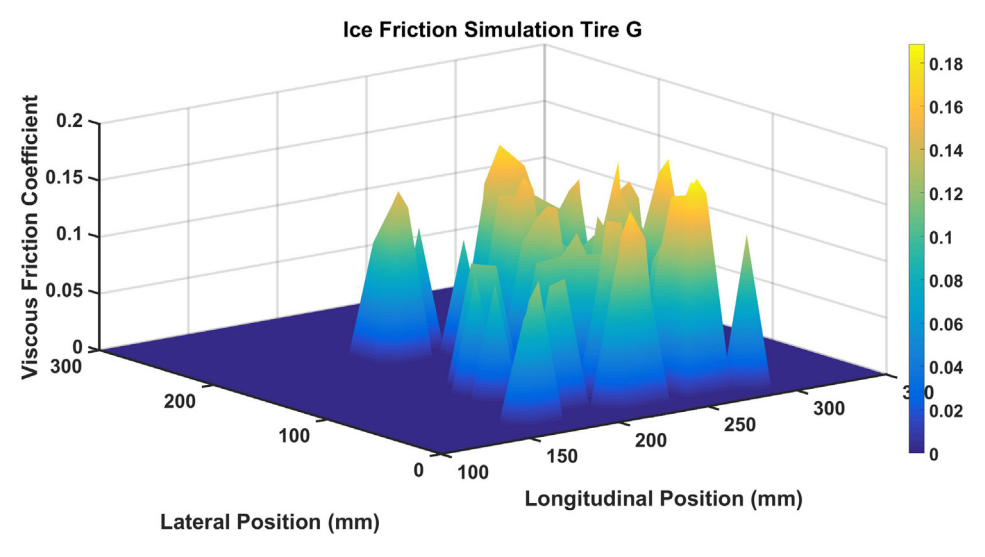


Fig. 35. Viscous friction coefficient in the contact patch for tire G for the braking condition, modeled by ATIIM2.0.

Table 2Comparison between parameters obtained by ATIIM2.0 for tires B, C, and G for the braking condition.

	Tire B	Tire C	Tire G
Avg viscous friction coefficient	0.21	0.17	0.13
Avg dry friction coefficient	0.28	0.30	0.3
Avg total friction coefficient	0.28	0.28	0.26
Avg temperature change in wet region [°C]	1.1	1	1.1
Area of wet region [m ²]	0.00388	0.00459	0.00579
Area of contact patch [m ²]	0.0257	0.0269	0.0267

As it can be seen from Table 3, three tire B, C, and G were chosen for the experimental study. Two levels of normal load were applied on the tires. For the first set of tests, the tire temperature was set at $-10\,^{\circ}\mathrm{C}$ when the applied normal load was at 5.6 kN, and the inflation pressure was kept at 193 kPa. For the next set of tests, the temperature of the tire increased to $-5\,^{\circ}\mathrm{C}$ while the rest of the parameters were kept constant. For the last set of tests, the tire temperature and ice temperature increased to $-1\,^{\circ}\mathrm{C}$ while the normal load and the inflation pressure decreased to 4 kN and 144.8 kPa, respectively.

The experimental results can be divided into three categories: 1. The tires were at $-10\,^{\circ}\text{C}$, under 5.6 kN normal load, at 193 kPa inflation pressure, and the ice temperature was $-10\,^{\circ}\text{C}$; 2. The tires were at $-5\,^{\circ}\text{C}$, under 5.6 kN normal load, at 193 kPa inflation pressure, and the ice temperature was $-10\,^{\circ}\text{C}$; 3. The tires were at $-1\,^{\circ}\text{C}$, under 4 kN normal load, at 144.8 kPa inflation pressure, and the ice temperature was $-1\,^{\circ}\text{C}$ for. The slip ratio was set at the same specific values used in the simulation, in the range of 2% to 15% and the camber and toe angles were equal to zero during all the tests.

In order to monitor the temperature changes at the contact patch, eight thermocouples were mounted on each tire. The ice surface was prepared frequently to maintain the constant desired value (μ = 0.1) for the friction coefficient test in order to ensure consistency during the tests. However, it has to be mentioned that this friction coefficient value measured by the tool available in the lab provides generic information about the ice surface preparation, but the apparatus is not able nor designed for measuring icerubber friction for different types of rubber, so the value measured cannot represent the friction coefficient at the contact patch for each tire tested precisely.

The slip ratio was applied to the Terramechanics Rig by changing the angular velocity of the wheel motor of the RIG according to Eq. (27), (He et al., 2019). The linear speed was kept constant.

$$S = \frac{R_e \omega - V}{V} \tag{30}$$

where ω is the angular speed of the tire, S is the slip ratio, R_e is the effective rolling radius of the tire, and V is the longitudinal speed of the carriage.

A proportional valve and a PID controller were used to control the applied normal load on the tire. The value of drawbar pull coefficient has been obtained in order to remove the effect of small fluctuations in the normal load. The drawbar pull coefficient =

$$\frac{F_X}{FZ}$$
 (31)

where F_Z is the normal load on the tire and F_X is the longitudinal force measured by Kistler sensor.

Fig. 36 shows the results for the drawbar pull coefficient of all three tires for two of the tested condition: a. Tires at -10 °C, 5.6 kN normal load, and 193 kPa inflation pressure in contact with ice at -10 °C, and b. Tires at -1 °C, 4 kN normal load, and 144.8 kPa in contact with ice at -1 °C. As it can be seen from Fig. 36, tire B had the highest drawbar pull for both conditions.

Table 3Design of experiment for the study on the tread rubber compound effect on tire performance on ice.

Tire	Tire B		Tire C	Tire C		Tire G	
Normal load	4 kN	5.6 kN	4 kN	5.6 kN	4 kN	5.6 kN	
Inflation pressure	144.8 kPa	193 kPa	144.8 kPa	193 kPa	144.8 kPa	193 kPa	
Tire temperature	−1 °C	-10 °C, −5 °C	−1 °C	-10 °C, −5 °C	−1 °C	-10 °C, −5 °C	
Ice temperature	−1 °C	−10 °C	−1 °C	−10 °C	−1 °C	−10 °C	
Slip ratio	0%, 2%, 4%, 8%, 12%, 15%, 20%, 30%						
Driving mode	Free rolling, braking, and traction						
Pressure distribution measurement	Pressure distribution at the contact patch was measured for each case						

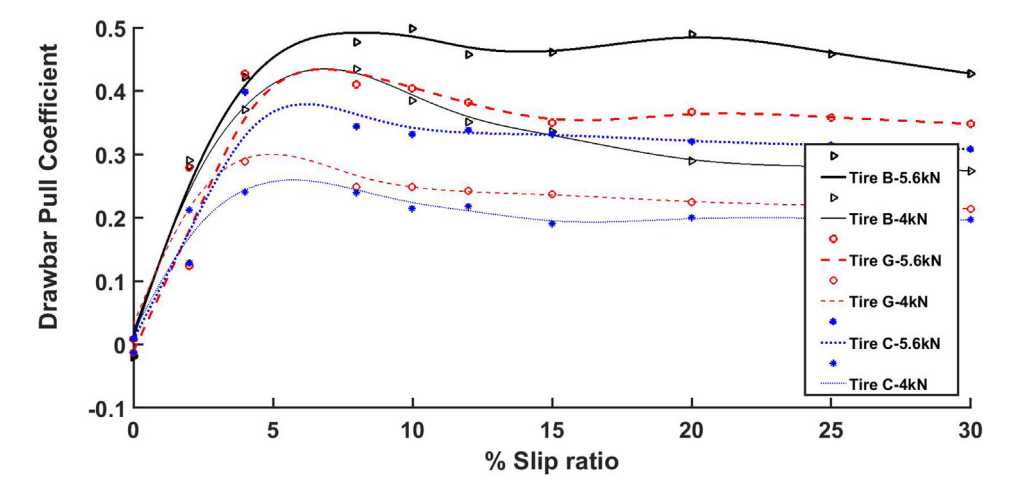


Fig. 36. Drawbar pull coefficient for tires B, C, and G for two conditions: a. Tires at -10 °C, 5.6 kN normal load, and 193 kPa inflation pressure in contact with ice at -10 °C, and b. Tires at -1 °C, 4 kN normal load, and 144.8 kPa in contact with ice at -1 °C.

The study of the traction performance of the tires B, C, and G is important, and the simulation results show the sensitivity of the magnitude of the drawbar pull to different tire parameters, such as normal load and ice temperature. However, as the ATIIM2.0 focuses on the prediction of the tire frictional force, to validate the simulation results using experimental data, we used the results for all tires during the free rolling tests. When the tire is in free rolling, the only force applied on the tire is the frictional force. Thus, the longitudinal forces collected by the Kistler sensor come only from this frictional force. As it has been presented in the publication describing the experimental study conducted for the effect of rubber compound on tire performance, (Mousavi and Sandu, 2020b; Mousavi et al., 2019; Mousavi and Sandu, 2020a), the value of the frictional force for tire B is higher than for Tire C. Tire G has the lowest value of the friction force. These results are very well correlated with the experimental results for the frictional force of the tires, thus validating the ATIIM2.0.

6. Conclusion

The purpose of this study is to enhance the understanding of the tire-ice contact interaction at the contact patch using a semiempirical the improved Advanced Tire-Ice Interface Model (ATIIM2.0) for a pneumatic tire traversing over solid ice.

In order to achieve the goal of this study, the advanced tire-ice interface model (ATIIM) has been improved to account for more material properties of the tread rubber. In addition, the improved model is suitable for predicting the tire-ice friction for both, wet and try contact. Simulation results from ATIIM2.0 for different scenarios were presented to illustrate the effects of different rubber compounds on tire performance. From the results obtained by ATIIM2.0:

- The values of the average friction coefficient obtained using ATIIM2.0 for tires B, C, and G are close to the measured static friction coefficient (~0.1).
- Tire B has the highest value of viscous, dry, and total friction coefficient; tire C has the next highest value. These results match with the experimental results for the free rolling test (that is related only to the resistive force of the tire).
- According to the results from the experiment, tire B, which has
 the smallest E modulus, has the highest friction coefficient for
 both, simulation and experiment. Further study is required to
 claim the fact by increasing the E modulus of the rubber, the
 value of the average viscous friction coefficient decreases.

According to the experimental and simulation results, tire B that has the smallest specific heat parameter among the three tires tested expressed the largest friction coefficient. These results give us the idea of increasing the specific heat of the rubber will decrease the value of the average viscous friction coefficient. However, further studies are required to prove this idea.

From the results for the braking condition of the tires obtained using ATIIM2.0, tire B has the highest value of the viscous friction coefficient. Similar to the results obtained experimentally, tire C has the next highest value. Further research is still required to investigate the correlations between rubber compound properties and tire performance.

Declaration of Competing Interest

The authors declare that they have no known competing financial interests or personal relationships that could have appeared to influence the work reported in this paper.

Acknowledgments

The authors would like to thank TMVS lab for the testing facilities used in this study and the support of the NSF I/UCRC Center for Tire Research (CenTiRe), who partially funded this work. The authors also would like to thank Mr. Mehran Shams for his help during this study, and Mr. Mohit Nitin Shenvi for his help in conducting the tests for the experimental study.

References

- Bhoopalam, A.K., Sandu, C., Taheri, S., 2016. A tire-ice model (TIM) for traction estimation. J. Terramech. 66, 1–12. https://doi.org/10.1016/j.jterra.2016.02.003.
- Bhoopalam, A.K., Sandu, C., Taheri, S., 2015a. Experimental investigation of the performance of pneumatic tires on ice. Part I - Indoor study. J. Terramech 60, 43–54. https://doi.org/10.1016/j.jterra.2015.02.006.
- Bhoopalam, A.K., Sandu, C., Taheri, S., 2015b. Experimental investigation of the performance of pneumatic tires on ice. part II Outdoor Study. J. Terramech. 60, 55–62. https://doi.org/10.1016/j.jterra.2015.03.001.
- Bhoopalam, A.K., Sandu, C., Taheri, S., 2014. Tire traction of commercial vehicles driving on icy roads. SAE Int. J. Commercial Vehicles 7 (2), 357–365. https://doi.org/10.4271/2014-01-2292.
- Fujikawa, T., Funazaki, A., Yamazaki, S., 1994. Tire tread temperatures in actual contact areas. Tire Sci. Technol. 22 (1), 19–41.
- Gießler, Martin, Frank, K., Wiese, Gauterin, Wies, B., 2010. Influence of friction heat on tire traction on ice and snow. Tire Sci. Technol. 38 (1), 4–23.
- He, R., Shenvi, M. N., Mousavi H., Sandu, C. et al. 2019. Updates of international society for terrain-vehicle systems standards. In: Proceedings of the 15th ISTVS European-African Regional Conference, Czech Republic, Prague.
- Ivanovic, V., Deur, J., Kostelac, M., Herold, Z., et al., 2006. Experimental identification of dynamic tire friction potential on ice surfaces. Veh. Syst. Dyn. 44, 93–103. https://doi.org/10.1080/00423110600869230.
- Jaeger, J. C., 1942. Moving sources of heat and the temperature of sliding contacts. In: Proceedings of the royal society of New South Wales, vol. 76, 203-224.
- Jimenez, E., Sandu, C., 2019. Towards a real-time pneumatic tire performance prediction using an advanced tire-ice interface model. J. Terramech. 81, 43-56. https://doi.org/10.1016/j.jterra.2018.04.004.
- Jimenez, E., Sandu, C., 2018. Experimental investigation of the tractive performance of pneumatic tires on ice. Tire Sci. Technol.
- Kandeva, M., Dishovsky, N., 2019. Friction behavior produced in the course of a contact enabled between composite materials and eco-friendly soles prototypes made of elastomeric material with regard to ice-covered surface. Tribol. Ind. 41, 90–99 https://doi.org/10.24874/ii.2019.41.01.10.
- Khan, A. K., Sandu, C., 2017. Design and manufacturing of a clutch and brake system for indoor tire testing. In ASME 2017 International Design Engineering Technical Conferences and Computers and Information in Engineering Conference. American Society of Mechanical Engineers Digital Collection.
- Liang, C., Ji, L., Mousavi, H., Sandu, C., 2019. Evaluation of tire traction performance on dry surface based on tire-road contact stress. In: SIAR International Congress of Automotive and Transport Engineering. Science and Management of Automotive and Transportation Engineering, 138–152. https://doi.org/ 10.1007/978-3-030-32564-0_17.
- Makkonen, L., Tikanmäki, M., 2014. Modeling the friction of ice. Cold Reg. Sci. Technol. 102, 84–93. https://doi.org/10.1016/j.coldregions.2014.03.002.
- Mashhadi, B., Mousavi, H., Montazeri, M., 2015. Obtaining relations between the Magic Formula coefficients and tire physical properties. Int. J. Automot. Eng. 5, 911–922.
- Mousavi, H., Shenvi, M.N., Sandu, C., 2019. Experimental study for free rolling of tire on ice. ASME 2019 Int. Des. Eng. Tech. Conf. Comput. Inf. Eng. Conf. IDETC/CIE 2019, 1–11. https://doi.org/10.1115/DETC2019-97846.
- Mousavi, H., Sandu, C., 2020. Study on the effects of rubber compounds on tire performance on ice. SAE Tech. Pap., 2020-01-1228, e-ISSN, 2688-3627. https://doi.org/10.4271/2020-01-1228.
- Mousavi, H., Sandu, C., 2020b. Experimental Study of Tread Rubber Compound Effects on Tire Performance on Ice. SAE Int. J. Commer. Veh. 13 (2). https://doi.org/10.4271/02-13-02-0006.
- Peng, X.D., Xie, Y.B., Guo, K.H., 2000. A new method for determining tire traction on ice. SAE Tech. Pap. https://doi.org/10.4271/2000-01-1640.
- Pressure Mapping Sensor 3150, https://www.tekscan.com/products-solutions/pressure-mapping-sensors/3150, (accessed March 2019)
- Roberts, A.D., 1981. Rubber-ice adhesion and friction. J. Adhesion 13 (1), 77–86.
- Sandu, C., Taylor, B., Biggans, J., and Ahmadian, M., 2008. Building an infrastructure for indoor terramechanics studies: the development of a terramechanics rig at Virginia Tech. In: Proceedings of 16th ISTVS international conference, Turin, Italy, pp. 177–85.
- Savitski, D., Schleinin, D., Ivanov, V., Augsburg, K., et al., 2017. Improvement of traction performance and off-road mobility for the vehicle with four individual electric motors: driving over icy road. J. Terramech. 69, 33–43. https://doi.org/ 10.1016/j.jterra.2016.10.005.
- Wiese, K., Kessel, T.M., Mundl, R., Wies, B., 2012. An analytical thermodynamic approach to friction of rubber on ice. Tire Sci. Technol. 40, 124–150.